Supplementary Information

for the manuscript

Sorption kinetics of metallic and organic contaminants on micro- and nanoplastics: remarkable dependence of the intraparticulate contaminant diffusion coefficient on particle size and potential role of polymer crystallinity

Raewyn M. Town[a]*, Herman P. van Leeuwen[a], Jérôme F.L. Duval[b*]

[a]ECOSPHERE, Department of Biology, Universiteit Antwerpen, Groenenborgerlaan 171, 2020 Antwerpen, Belgium. Corresponding author, e-mail: raewyn.town@uantwerpen.be

[b]Université de Lorraine, CNRS, LIEC, F-54000 Nancy, France. Corresponding author, e-mail: jerome.duval@univ-lorraine.fr

This document contains 40 pages, 16 figures, 11 equations, 1 Table and a glossary of symbols.

All references mentioned here are reported at the end of the document, p. 38-40.

Glossary of symbols

Latin

a Radius of plastic particle

$c_{\mathrm{X,w}}\left(a<r\le r_{\mathrm{c}},t\right)$ Concentration profile of contaminant X at time *t* in the extraparticulate aqueous medium

$c_{\mathrm{X,p}}\left(0\le r\le a,t\right)$ Intraparticulate concentration profile of contaminant X at time *t*

$\overline{c}_{\mathrm{X,p}}$ Dimensionless intraparticulate concentration of contaminant X defined by $c_{\mathrm{X,p}}$ / $c_{\mathrm{X,p}}^{\mathrm{norm;i=H,L,LF}}$

$c_{\mathrm{X,w}}^{*}\left(t\right)$ Bulk medium concentration of contaminant X at time *t*

$\overline{c}_{\mathrm{X,w}}^{*}$ Dimensionless bulk medium concentration of contaminant X defined by $c_{\mathrm{X,w}}^{*}$ / $c_{\mathrm{X,w}}^{*}\left(t=0\right)$

$c_{\mathrm{X,w}}^{*,0}=c_{\mathrm{X,w}}^{*}\left(t=0\right)$ Initial bulk medium concentration of contaminant X

$c_{\mathrm{X,p}}^{\mathrm{max,s}}$ Maximum surface sorption capacity of contaminant X (relevant for Langmuir and Langmuir-Freundlich isotherms)

$c_{\mathrm{X,w}}^{*,\mathrm{eq}}=c_{\mathrm{X,w}}^{*}\left(t\to\infty\right)$ Bulk medium concentration of contaminant X at equilibrium

$c_{\mathrm{X,p}}^{\mathrm{norm;i=H,L,LF}}$ Concentrations defined by $c_{\mathrm{X,p}}^{\mathrm{norm;i=H}}=K_{\mathrm{p,w}}^{\mathrm{H}}c_{\mathrm{X,w}}^{*,0}$ and $c_{\mathrm{X,p}}^{\mathrm{norm;i=L,LF}}=c_{\mathrm{X,p}}^{\mathrm{max,s}}$

$\overline{c}_{\mathrm{X,p}}\left(\overline{r},\overline{t}=\overline{t}_{k}\right)=\overline{c}_{\mathrm{X,p}}^{(k)}\left(\overline{r}\right)$ (Discretized) Dimensionless intraparticulate concentration taken at the reduced space and time variables $\overline{r}=r/a$ ($0\le\overline{r}\le1$) and $\overline{t}=t/\left(\beta\tau\right)$ ($0\le\overline{t}\le1$), respectively

$\overline{c}_{\mathrm{X,w}}^{*}\left(\overline{t}=\overline{t}_{k}\right)=\overline{c}_{\mathrm{X,w}}^{(k)}$ (Discretized) Dimensionless extraparticulate bulk concentration taken at the reduced time variable $\overline{t}=t/\left(\beta\tau\right)$ ($0\le\overline{t}\le1$)

$C_{\mathrm{X,p}}\left(t\right)$ Intraparticulate concentration of contaminant X at time *t*

$C_{\mathrm{X,p}}^{\mathrm{eq}}=C_{\mathrm{X,p}}\left(t\to\infty\right)$ Intraparticulate concentration of contaminant X at equilibrium

$D_{\mathrm{X,p}}$ Intraparticulate diffusion coefficient of contaminant X

$D_{\mathrm{X,w}}$ Diffusion coefficient of contaminant X in the extraparticulate aqueous medium

$f_{\mathrm{i=H,L,LF}}\left(c_{\mathrm{X,w}}^{*}\left(t\right)\right)$ Isotherm defined by eqns (1-2a) (i=H), (1-2b) (i=L) and (1-2c) (i=LF)

$K_{\mathrm{p,w}}^{\mathrm{H}}$ Henry partition coefficient of contaminant X at the particle/water interface

$K_{\mathrm{p,w}}^{\mathrm{L}}$ Langmuir partition coefficient of contaminant X at the particle/water interface

$K_{\mathrm{p,w}}^{\mathrm{LF}}$ Langmuir-Freundlich partition coefficient of contaminant X at the particle/water interface

$1/p_{\mathrm{LF}}$ Heterogeneity parameter involved in the Langmuir-Freundlich isotherm

r Radial coordinate (Fig. 1)

$\overline{r}=r/a$ Dimensionless (or reduced) radial coordinate

r_{c} Radius of the Kuwabara cell (Fig. 1)

t Time

$\overline{t}=t/\left(\beta\tau\right)$ Dimensionless (or reduced) time variable

$\bar{t}_k = (k-1)\Delta\bar{t}$ Discretized time with *k* an integer running from 1 to $N >> 1$

V_p Particle volume

Greek

β Dimensionless scalar chosen to cover a prescribed range of time values *t*

φ Particle volume fraction

$\tau = a^2 / D_{X,p}$ Characteristic intraparticulate diffusion timescale of contaminant X

$\Delta\bar{t} = 1/(N-1)$ Time step in the discretization procedure adopted to solve eqns (1-8).

Supplementary details on numerical analysis

Following the approach specified in the main text, the dimensionless forms of eqns (1-2) for Henry, Langmuir and Langmuir-Freundlich isotherms are given by

$$\bar{c}_{X,p}(\bar{r}=1,\bar{t}) = \bar{c}^*_{X,w}(\bar{t}) \tag{S1a}$$

$$\bar{c}_{X,p}(\bar{r}=1,\bar{t}) = \frac{K^L_{p,w} c^{*,0}_{X,w} \bar{c}^*_{X,w}(\bar{t})}{1 + K^L_{p,w} c^{*,0}_{X,w} \bar{c}^*_{X,w}(\bar{t})} \tag{S1b}$$

$$\bar{c}_{X,p}(\bar{r}=1,\bar{t}) = \frac{\left(K^{LF}_{p,w} c^{*,0}_{X,w} \bar{c}^*_{X,w}(\bar{t})\right)^{1/p_{LF}}}{1 + \left(K^{LF}_{p,w} c^{*,0}_{X,w} \bar{c}^*_{X,w}(\bar{t})\right)^{1/p_{LF}}} \tag{S1c}$$

, respectively, where $\bar{r} = r/a$ $(0 \le \bar{r} \le 1)$, $\bar{t} = t/(\beta\tau)$ $(0 \le \bar{t} \le 1)$ with $\tau = a^2 / D_{X,p}$ (s) and β a factor (dimensionless) chosen for *t* to cover a range of desired values, $\bar{c}^*_{X,w}(\bar{t}) = c^*_{X,w}(\bar{t}) / c^{*,0}_{X,w}$ and $\bar{c}_{X,p}(\bar{r},\bar{t}) = c_{X,p}(\bar{r},\bar{t}) / c^{norm;i=H,L,LF}_{X,p}$, with $c^{norm;i=H,L,LF}_{X,p}$ defined by $c^{norm;i=H}_{X,p} = K^H_{p,w} c^{*,0}_{X,w}$ and $c^{norm;i=L,LF}_{X,p} = c^{max,s}_{X,p}$. The dimensionless form of the transient Fick diffusion eqn (3) is further simply written

$$\frac{\partial \bar{c}_{X,p}(\bar{r},\bar{t})}{\partial \bar{t}} = \beta\left[\frac{\partial^2 \bar{c}_{X,p}(\bar{r},\bar{t})}{\partial \bar{r}^2} + \frac{2\gamma}{\bar{r}} \frac{\partial \bar{c}_{X,p}(\bar{r},\bar{t})}{\partial \bar{r}}\right] \tag{S2}$$

and the dimensionless boundaries derived from eqns (4-5) are

$$\bar{c}_{X,p}(0 \le \bar{r} \le 1, \bar{t} = 0) = 0 \tag{S3}$$

and

$$\left.\frac{\partial \bar{c}_{X,p}(\bar{r},\bar{t})}{\partial \bar{r}}\right|_{\bar{r}=0} = 0 \tag{S4}$$

, respectively. Finally, the dimensionless form of the mass balance condition (eqn (7)) is given by

$$\frac{\mathrm{d}\bar{c}^{*}_{\mathrm{X,w}}\left(\bar{t}\right)}{\mathrm{d}\bar{t}} = -\frac{3\varphi}{1-\varphi}\beta\frac{c^{\mathrm{norm;i=H,L,LF}}_{\mathrm{X,p}}}{c^{*,0}_{\mathrm{X,w}}}\left.\frac{\partial\bar{c}_{\mathrm{X,p}}\left(\bar{r},\bar{t}\right)}{\partial\bar{r}}\right|_{\bar{r}=1} \tag{S5}$$

Introducing the discretized and dimensionless concentrations $\bar{c}_{\mathrm{X,p}}\left(\bar{r},\bar{t}=\bar{t}_k\right)=\bar{c}^{(k)}_{\mathrm{X,p}}\left(\bar{r}\right)$ and $\bar{c}^{*}_{\mathrm{X,w}}\left(\bar{t}=\bar{t}_k\right)=\bar{c}^{(k)}_{\mathrm{X,w}}$ where the integer k runs from 1 to $N>>1$ and $\bar{t}_k=\left(k-1\right)\Delta\bar{t}$ pertains to the discretized time with $\Delta\bar{t}=1/\left(N-1\right)$, eqns (S1-S5) becomes after implicit Euler discretization procedure

$$\bar{c}^{(k)}_{\mathrm{X,p}}\left(\bar{r}=1\right)=\bar{c}^{(k)}_{\mathrm{X,w}} \quad \text{for } k=2,\ldots,N \tag{S6a}$$

$$\bar{c}^{(k)}_{\mathrm{X,p}}\left(\bar{r}=1\right)=\frac{K^{\mathrm{L}}_{\mathrm{p,w}}c^{*,0}_{\mathrm{X,w}}\bar{c}^{(k)}_{\mathrm{X,w}}}{1+K^{\mathrm{L}}_{\mathrm{p,w}}c^{*,0}_{\mathrm{X,w}}\bar{c}^{(k)}_{\mathrm{X,w}}} \quad \text{for } k=2,\ldots,N \tag{S6b}$$

$$\bar{c}^{(k)}_{\mathrm{X,p}}\left(\bar{r}=1\right)=\frac{\left(K^{\mathrm{LF}}_{\mathrm{p,w}}c^{*,0}_{\mathrm{X,w}}\bar{c}^{(k)}_{\mathrm{X,w}}\right)^{1/p_{\mathrm{LF}}}}{1+\left(K^{\mathrm{LF}}_{\mathrm{p,w}}c^{*,0}_{\mathrm{X,w}}\bar{c}^{(k)}_{\mathrm{X,w}}\right)^{1/p_{\mathrm{LF}}}} \quad \text{for } k=2,\ldots,N \tag{S6c}$$

$$\frac{\partial^2\bar{c}^{(k)}_{\mathrm{X,p}}\left(\bar{r}\right)}{\partial\bar{r}^2}=\frac{1}{\beta\Delta\bar{t}}\left(\bar{c}^{(k)}_{\mathrm{X,p}}\left(\bar{r}\right)-\bar{c}^{(k-1)}_{\mathrm{X,p}}\left(\bar{r}\right)\right)-\frac{2\gamma}{\bar{r}}\frac{\partial\bar{c}^{(k)}_{\mathrm{X,p}}\left(\bar{r}\right)}{\partial\bar{r}} \quad \text{for } k=2,\ldots,N \tag{S7}$$

$$\bar{c}^{(k=1)}_{\mathrm{X,p}}\left(0\le\bar{r}\le1\right)=0 \tag{S8}$$

$$\left.\frac{\partial\bar{c}^{(k)}_{\mathrm{X,p}}\left(\bar{r}\right)}{\partial\bar{r}}\right|_{\bar{r}=0}=0 \quad \text{for } k=2,\ldots,N \tag{S9}$$

$$\bar{c}^{(k)}_{\mathrm{X,w}}=\bar{c}^{(k-1)}_{\mathrm{X,w}}-\frac{3\varphi}{1-\varphi}\beta\Delta\bar{t}\left.\frac{c^{\mathrm{norm;i=H,L,LF}}_{\mathrm{X,p}}}{c^{*,0}_{\mathrm{X,w}}}\frac{\partial\bar{c}^{(k)}_{\mathrm{X,p}}\left(\bar{r}\right)}{\partial\bar{r}}\right|_{\bar{r}=1} \quad \text{for } k=2,\ldots,N \tag{S10}$$

, respectively. We further recall the initial condition verified by the extraparticulate concentration

$$\bar{c}^{(k=1)}_{\mathrm{X,w}}=1 \tag{S11}$$

After solving $\left\{\bar{c}^{(k)}_{\mathrm{X,p}}\left(\bar{r}\right),\bar{c}^{(k)}_{\mathrm{X,w}}\right\}$ for $k=2,\ldots,N$ along the lines indicated in the main text, the kinetics of X sorption, $C_{\mathrm{X,p}}\left(t=t_{k=1,\ldots,N}\right)$, was evaluated by eqn (8) in the main text with the spatial integral therein estimated by the rectangle method.

Supplementary details on the strategy for fitting X isotherm and X sorption kinetic data (Fig. S1)

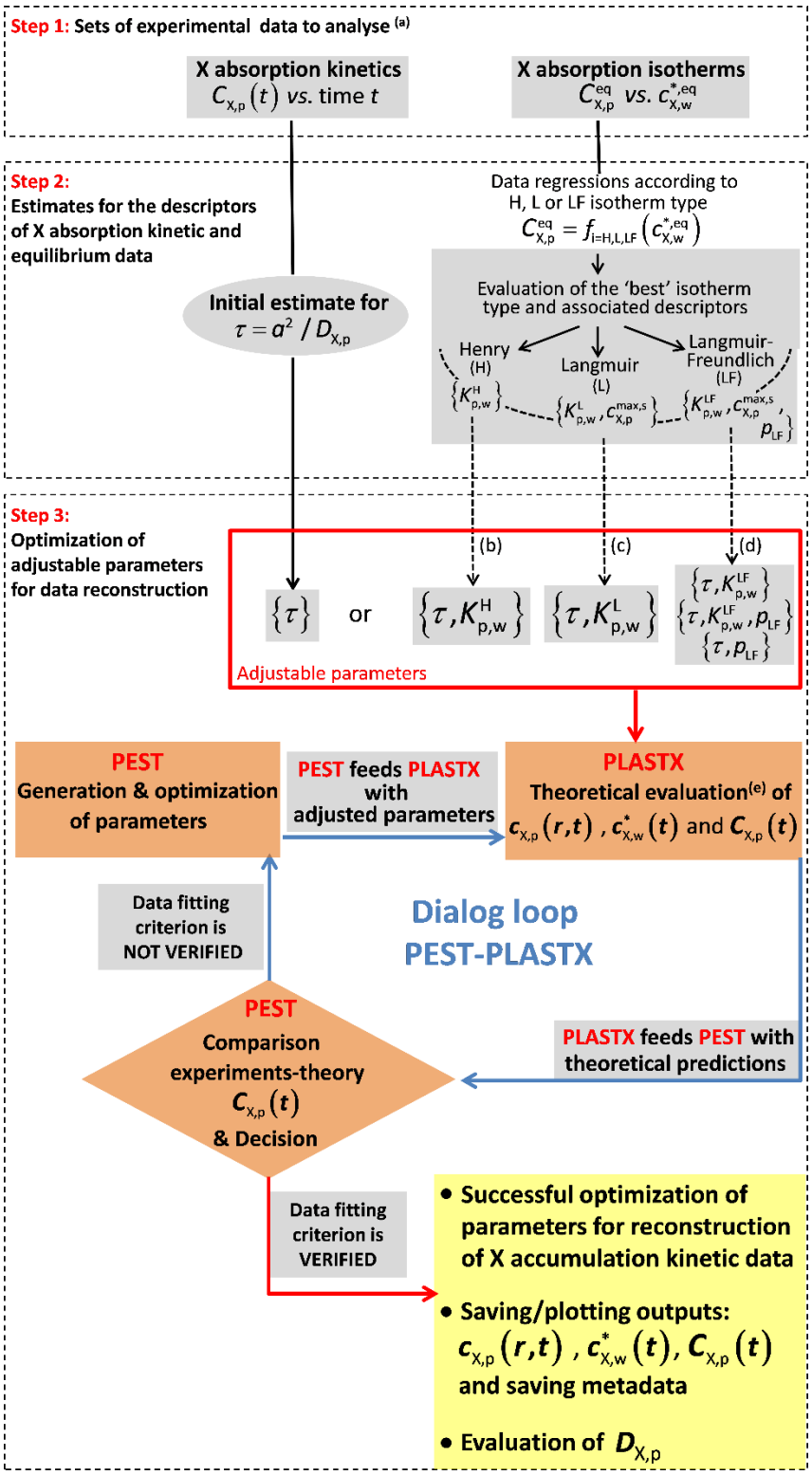

Fig. S1. Flowchart showing the steps involved in implementing the algorithm for the data fitting. Step 1 **(a)** Sufficiently documented literature data were selected for which both equilibrium isotherm and sorption kinetics were reported for pristine plastic particles of spherical or approximately spherical geometry. Studies were excluded from consideration if (i) the particle size was not reported or only poorly documented, (ii) only kinetic data were given, i.e. no corresponding equilibrium isotherms, (iii) very few time points were reported, and (iv) there were gross inconsistencies between the kinetic and equilibrium data. Once a good description of the equilibrium isotherm data was obtained (Step 2), PEST and PLASTX were run (Step 3) to fit the kinetic

sorption data with τ as the only adjustable parameter (and the values of the isotherm descriptors fixed at those determined from the independent equilibrium data and γ = 1 (spherical diffusion)); if the fit to the kinetic data was unsatisfactory, the PEST fitting was repeated with the equilibrium isotherm descriptors also adjustable according to the options specified in **(b), (c)** and **(d)** for the pertaining isotherms, and if the fit remained unsatisfactory the PEST fitting was repeated with γ = 0 (linear diffusion). **Table S1** documents the parameters that were adjusted for each data set. **(e)** Theoretical evaluation of eqns (1-8) (or, equivalently, eqns (S1-S5) or eqns (S6-S11)) along the lines indicated in the main text.

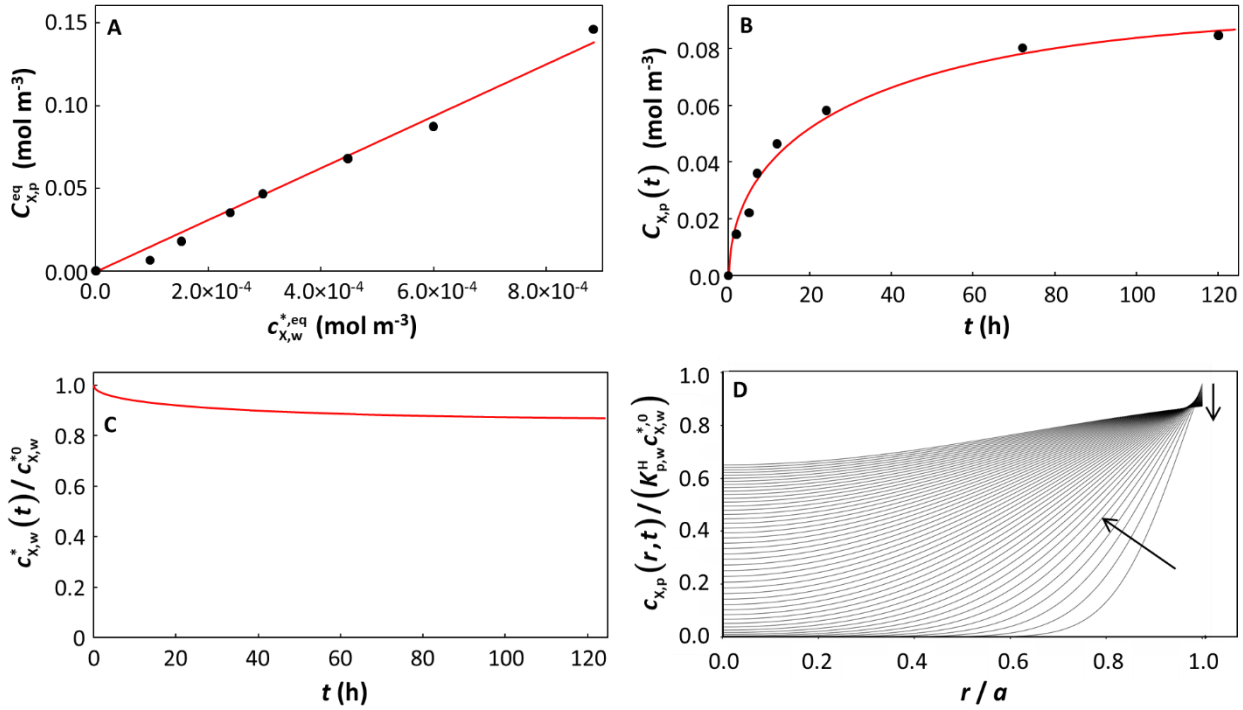

Fig. S2. Equilibrium and kinetic features of a system with low depletion of X in the bulk solution, linear (Henry) isotherm, $K^{H}_{p,w}$ fixed during fitting of the kinetic data: sorption of triadimefon on polyvinylchloride particles (a = 3.75×10^{-5} m). The panels correspond to: **(A)** equilibrium sorption isotherm; **(B)** kinetic sorption curves; **(C)** corresponding solution depletion profile; and **(D)** temporal evolution of the normalized intraparticulate concentration profiles, with the direction of increasing time indicated by the arrow. In (D), the timescale between two plotted concentration profiles is $\Delta t =$ 8334 s, starting at $t = 8334$ s. The situation at $t = 0$ (not shown) corresponds to plastic particles free of contaminants and to the initial bulk medium condition $c^{*}_{X,w}(t=0) = c^{*,0}_{X,w}$. The Henry isotherm best described the equilibrium data and τ was the only parameter that was optimized to fit the sorption curves (see **Table S1** for the pertaining parameters). The isotherm curve (A) shows the experimental data (black circles)[1] and the best fit obtained according to the Henry sorption isotherm (eqns (1-2a), red curve, adjusted parameter: $K^{H}_{p,w}$); the kinetic sorption curve (B) shows the experimental data (black circles)[1] and the numerically computed values, eqns (1-2a,3-5,7-8) (red curve); the depletion profile (C) shows the values obtained from numerical computation, eqns (1-2a,3-5,7) (red curve). The maximal extent of bulk depletion is 13% in the kinetic sorption data, and from the fitted τ of 578.6 h the derived diffusion coefficient is $D_{X,p} = 6.75\times10^{-16}$ m^2 s^{-1}.

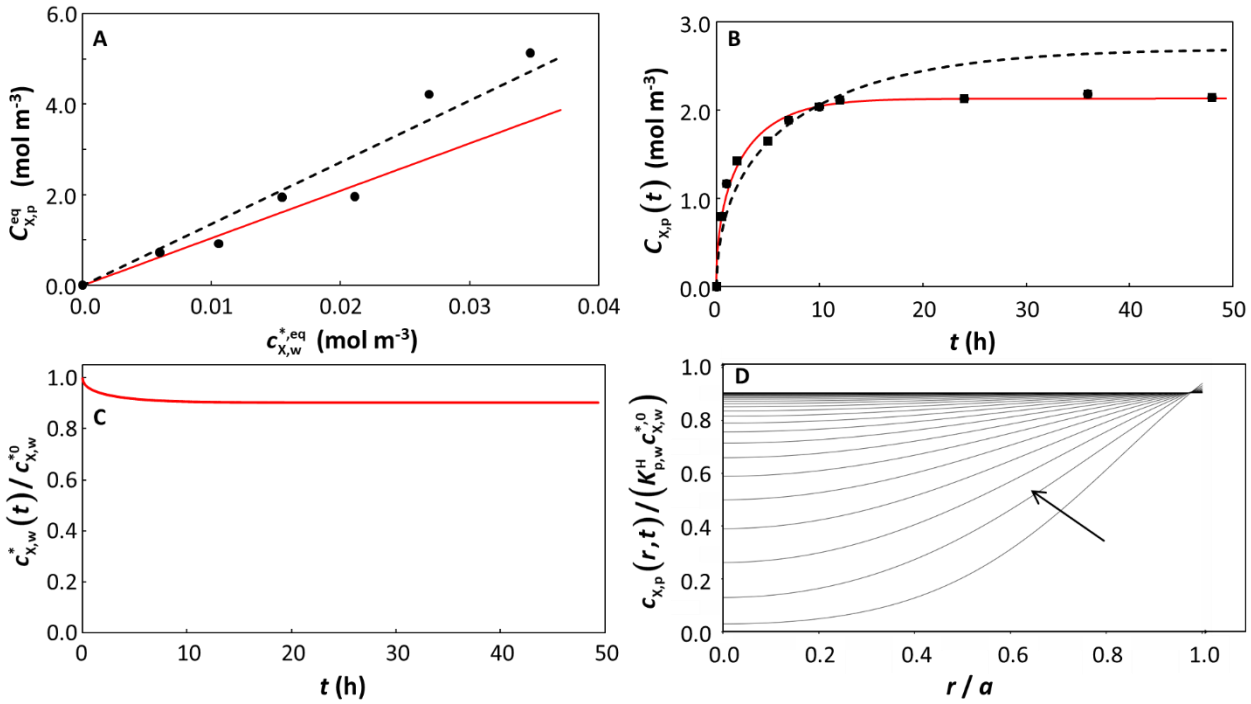

Fig. S3. Equilibrium and kinetic features of a system with low depletion of X in the bulk solution, linear (Henry) isotherm, $K^{H}_{p,w}$ varied during fitting of the kinetic data: sorption of tetracycline on polyvinylchloride particles (a = 4.0×10^{-5} m). The panels correspond to: **(A)** equilibrium sorption isotherm; **(B)** kinetic sorption curves; **(C)** corresponding solution depletion profile; and **(D)** temporal evolution of the normalized intraparticulate concentration profiles, with the direction of increasing time indicated by the arrow. In (D), the timescale between two plotted concentration profiles is $\Delta t =$ 3468 s, starting at $t = 3468$ s. The situation at $t = 0$ (not shown) corresponds to plastic particles free of contaminants and to the initial bulk medium condition $c^{*}_{X,w}(t=0) = c^{*,0}_{X,w}$. The Henry isotherm best described the equilibrium data and $K^{H}_{p,w}$ and τ were both optimized to fit the sorption curves (see **Table S1** for the pertaining parameters). The isotherm curve (A) shows the experimental data (black circles)[2] and the best fit obtained according to the Henry sorption isotherm (eqns (1-2a), black dashed curve, adjusted parameter: $K^{H}_{p,w}$), and the curve computed using the value of $K^{H}_{p,w}$ optimized during the kinetic fitting (red curve); the kinetic sorption curve (B) shows the experimental data (black circles)[2] and the numerically computed values using (i) the value of $K^{H}_{p,w}$ optimized during the kinetic fitting, eqns (1-2a,3-5,7-8) (red curve; $K^{H}_{p,w}$ = 104.8), and (ii) the value of $K^{H}_{p,w}$ fixed at the value determined from the equilibrium isotherm data (black dashed curve; $K^{H}_{p,w}$ = 136.4); the depletion profile (C) shows the values obtained from numerical computation, eqns (1-2a,3-5,7) (red curve). The maximal extent of bulk depletion is 9.5% in the kinetic sorption data, and from the fitted τ of 39.4 h the derived diffusion coefficient is $D_{X,p} = 1.13\times10^{-14}$ m^2 s^{-1}.

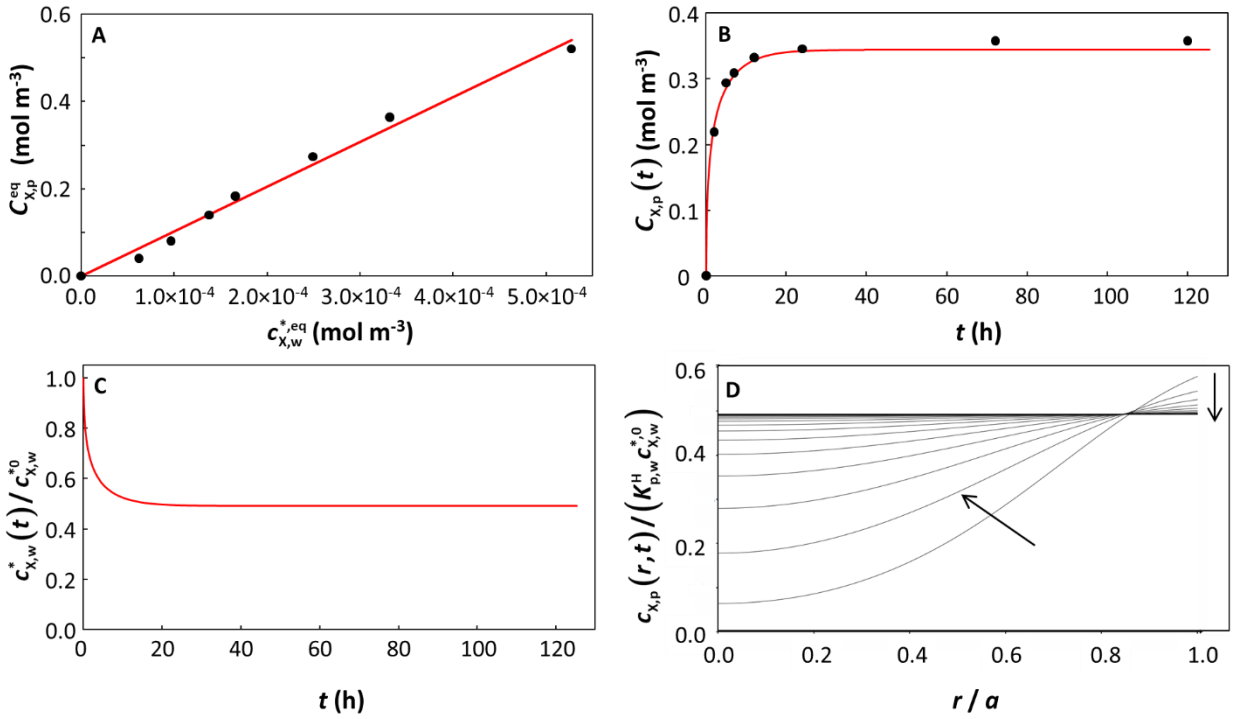

Fig. S4. Equilibrium and kinetic features of a system with significant depletion of X in the bulk solution, linear (Henry) isotherm, $K^{H}_{p,w}$ fixed during fitting of the kinetic data: sorption of triadimefon on PBS particles (a = 3.75×10^{-5} m). The panels correspond to: **(A)** equilibrium sorption isotherm; **(B)** kinetic sorption curves; **(C)** corresponding solution depletion profile; and **(D)** temporal evolution of the normalized intraparticulate concentration profiles, with the direction of increasing time indicated by the arrow. In (D), the timescale between two plotted concentration profiles is $\Delta t =$ 9025 s, starting at $t =$ 9025 s. The situation at $t = 0$ (not shown) corresponds to plastic particles free of contaminants and to the initial bulk medium condition $c^{*}_{X,w}(t=0) = c^{*,0}_{X,w}$. The Henry isotherm best described the equilibrium data and τ was the only parameter that was optimized to fit the sorption curves (see **Table S1** for the pertaining parameters). The isotherm curve (A) shows the experimental data (black circles)[1] and the best fit obtained according to the Henry sorption isotherm (eqns (1-2a), red curve, adjusted parameter: $K^{H}_{p,w}$); the kinetic sorption curve (B) shows the experimental data (black circles)[1] and the numerically computed values, eqns (1-2a,3-5,7-8) (red curve); the depletion profile (C) shows the values obtained from numerical computation, eqns (1-2a,3-5,7) (red curve). The maximal extent of bulk depletion is 51% in the kinetic sorption data, and from the fitted τ of 79.0 h the derived diffusion coefficient is $D_{X,p} = 4.94\times10^{-15}$ m^2 s^{-1}.

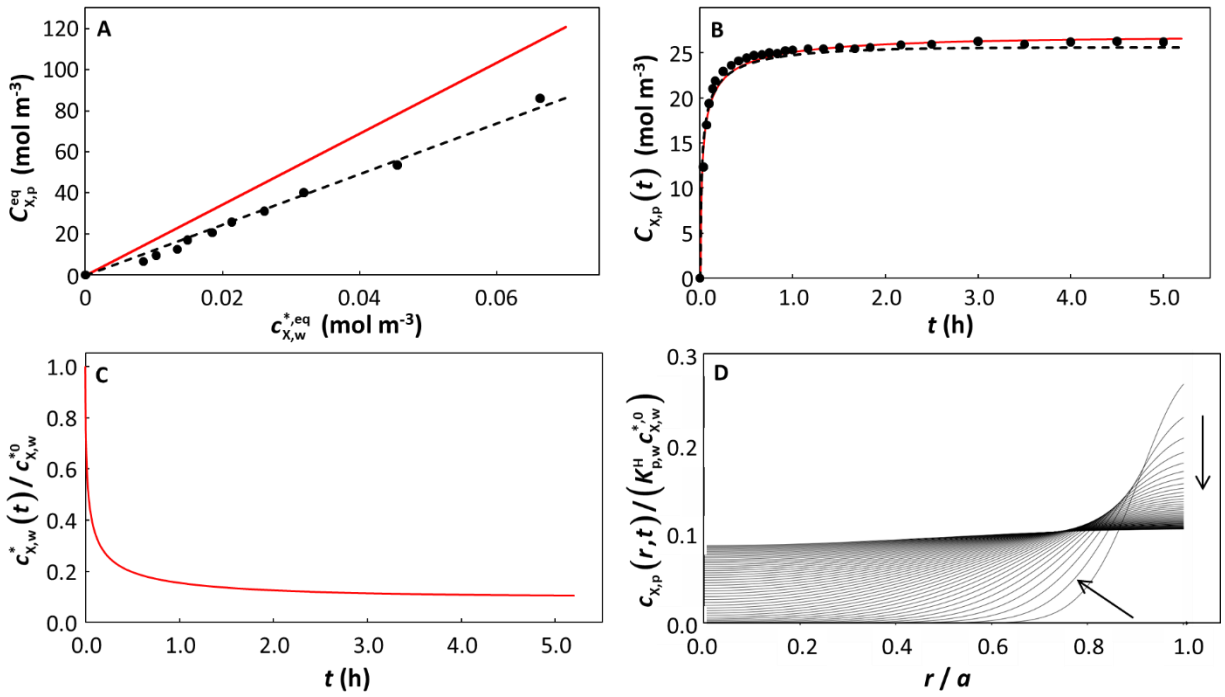

Fig. S5. Equilibrium and kinetic features of a system with significant depletion of X in the bulk solution, linear (Henry) isotherm, $K^{H}_{p,w}$ varied during fitting of the kinetic data: sorption of 1-methyl-naphthalene on polyethylene particles (a = 9.0×10^{-5} m). The panels correspond to: **(A)** equilibrium sorption isotherm; **(B)** kinetic sorption curves; **(C)** corresponding solution depletion profile; and **(D)** temporal evolution of the normalized intraparticulate concentration profiles, with the direction of increasing time indicated by the arrow. In (D), the timescale between two plotted concentration profiles is $\Delta t =$ 394 s, starting at $t = 394$ s. The situation at $t = 0$ (not shown) corresponds to plastic particles free of contaminants and to the initial bulk medium condition $c^{*}_{X,w}(t=0) = c^{*,0}_{X,w}$. The Henry isotherm best described the equilibrium data and $K^{H}_{p,w}$ and τ were both optimized to fit the sorption curves (see **Table S1** for the pertaining parameters). The isotherm curve (A) shows the experimental data (black circles)[3] and the best fit obtained according to the Henry sorption isotherm (eqns (1-2a), black dashed curve, adjusted parameter: $K^{H}_{p,w}$), and the curve computed using the value of $K^{H}_{p,w}$ optimized during the kinetic fitting (red curve); the kinetic sorption curve (B) shows the experimental data (black circles)[3] and the numerically computed values using (i) the value of $K^{H}_{p,w}$ optimized during the kinetic fitting, eqns (1-2a,3-5,7-8) (red curve; $K^{H}_{p,w}$ = 1726.8), and (ii) the value of $K^{H}_{p,w}$ fixed at the value determined from the equilibrium isotherm data (black dashed curve; $K^{H}_{p,w}$ = 1230.9); the depletion profile (C) shows the values obtained from numerical computation, eqns (1-2a,3-5,7) (red curve). The maximal extent of bulk depletion is 89% in the kinetic sorption data, and from the fitted τ of 34.0 h the derived diffusion coefficient is $D_{X,p} = 6.62\times10^{-14}$ m^2 s^{-1}.

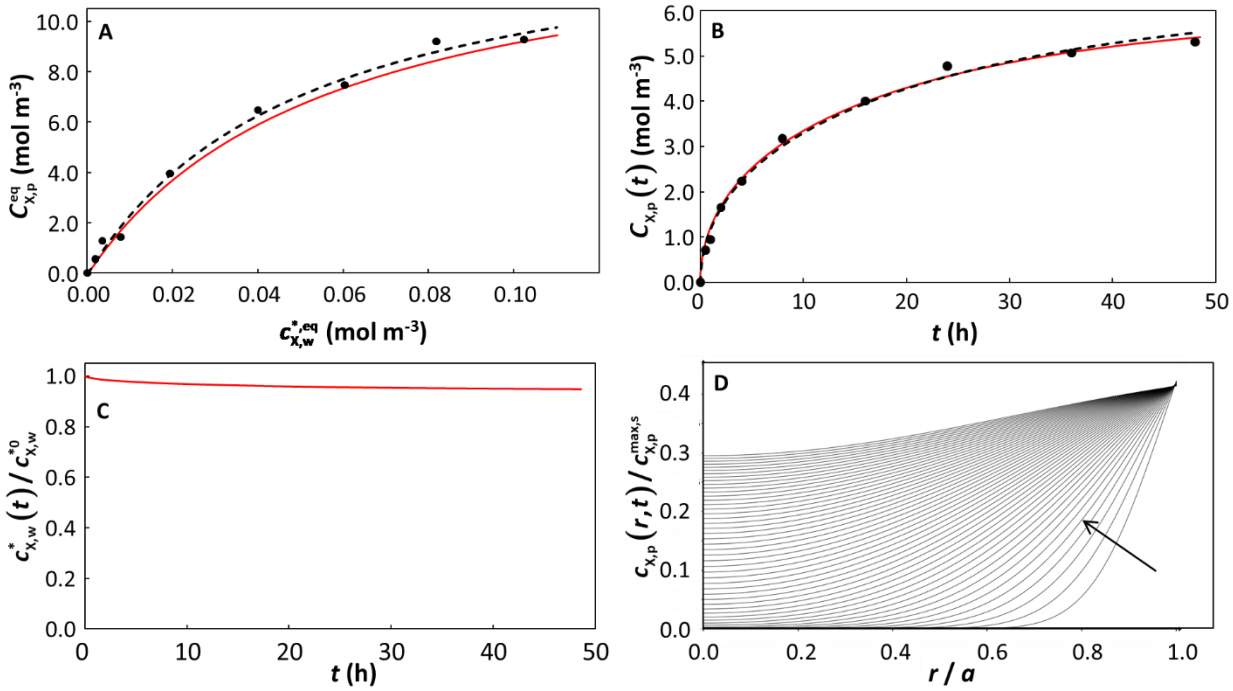

Fig. S6. Equilibrium and kinetic features of a system with low depletion of X in the bulk solution, Langmuir isotherm, $K^{L}_{p,w}$ varied during fitting of the kinetic data: sorption of carbamazepine on polystyrene particles (a = 4.6×10^{-5} m). The panels correspond to: **(A)** equilibrium sorption isotherm; **(B)** kinetic sorption curves; **(C)** corresponding solution depletion profile; and **(D)** temporal evolution of the normalized intraparticulate concentration profiles, with the direction of increasing time indicated by the arrow. In (D), the timescale between two plotted concentration profiles is $\Delta t = 3493$ s, starting at $t = 3493$ s. The situation at $t = 0$ (not shown) corresponds to plastic particles free of contaminants and to the initial bulk medium condition $c^{*}_{X,w}(t=0) = c^{*,0}_{X,w}$. The Langmuir isotherm best described the equilibrium data and $K^{L}_{p,w}$ and τ were both optimized to fit the sorption curves (see **Table S1** for the pertaining parameters). The isotherm curve (A) shows the experimental data (black circles)[4] and the best fit obtained according to the Langmuir sorption isotherm (eqns (1-2b), black dashed curve, adjusted parameter: $K^{L}_{p,w}$), and the curve computed using the value of $K^{L}_{p,w}$ optimized during the kinetic fitting (red curve); the kinetic sorption curve (B) shows the experimental data (black circles)[4] and the numerically computed values using (i) the value of $K^{L}_{p,w}$ optimized during the kinetic fitting, eqns (1-2b,3-5,7-8) (red curve; $K^{L}_{p,w}$ = 17.6 m^3 mol^{-1}), and (ii) the value of $K^{L}_{p,w}$ fixed at the value determined from the equilibrium isotherm data (black dashed curve; $K^{L}_{p,w}$ = 19.5 m^3 mol^{-1}); the depletion profile (C) shows the values obtained from numerical computation, eqns (1-2b,3-5,7) (red curve). The maximal extent of bulk depletion is 5% in the kinetic sorption data, and from the fitted τ of 248.9 h the derived diffusion coefficient is $D_{X,p} = 2.36\times10^{-15}$ m^2 s^{-1}.

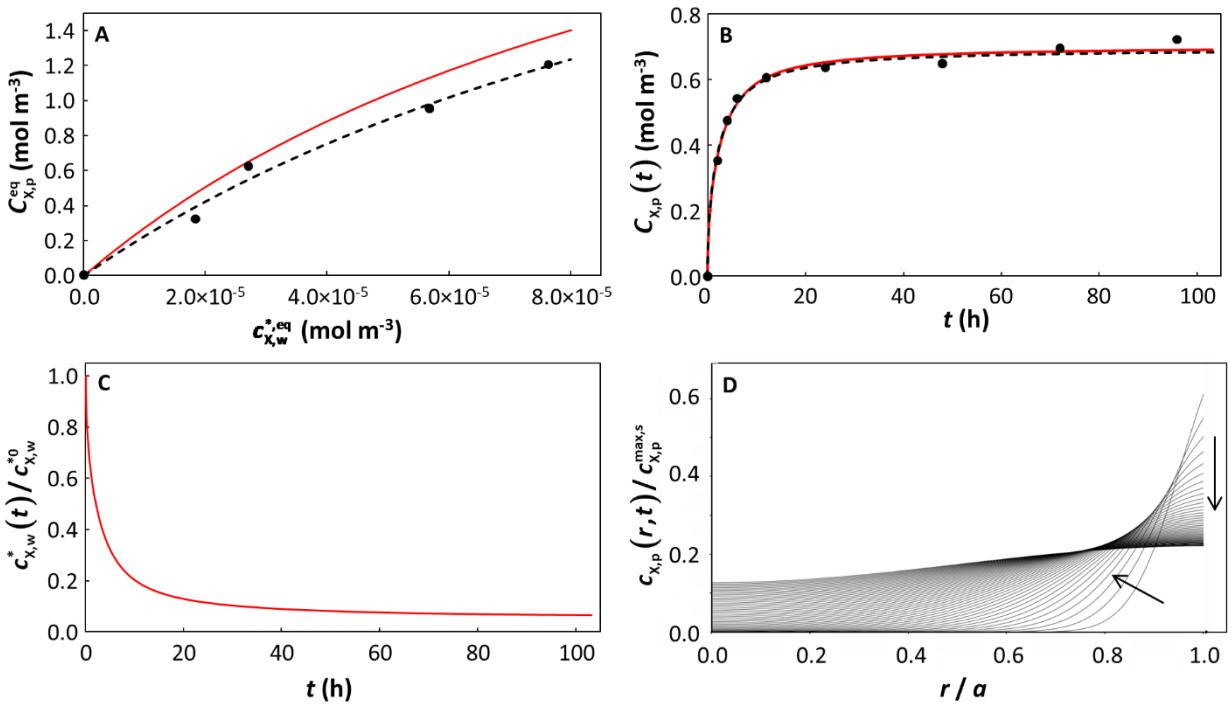

Fig. S7. Equilibrium and kinetic features of a system with significant depletion of X in the bulk solution, Langmuir isotherm, $K^{L}_{p,w}$ varied during fitting of the kinetic data: sorption of fluoranthene on polyethylene terephthalate particles (a = 1.5×10^{-3} m). The panels correspond to: **(A)** equilibrium sorption isotherm; **(B)** kinetic sorption curves; **(C)** corresponding solution depletion profile; and **(D)** temporal evolution of the normalized intraparticulate concentration profiles, with the direction of increasing time indicated by the arrow. In (D), the timescale between two plotted concentration profiles is $\Delta t = 7424$ s, starting at $t = 7424$ s. The situation at $t = 0$ (not shown) corresponds to plastic particles free of contaminants and to the initial bulk medium condition $c^{*}_{X,w}(t=0) = c^{*,0}_{X,w}$. The Langmuir isotherm best described the equilibrium data and $K^{L}_{p,w}$ and τ were both optimized to fit the sorption curves (see **Table S1** for the pertaining parameters). The isotherm curve (A) shows the experimental data (black circles)[5] and the best fit obtained according to the Langmuir sorption isotherm (eqns (1-2b), black dashed curve, adjusted parameter: $K^{L}_{p,w}$), and the curve computed using the value of $K^{L}_{p,w}$ optimized during the kinetic fitting (red curve); the kinetic sorption curve (B) shows the experimental data (black circles)[5] and the numerically computed values using (i) the value of $K^{L}_{p,w}$ optimized during the kinetic fitting, eqns (1-2b,3-5,7-8) (red curve; $K^{L}_{p,w}$ = 8730.4 m^3 mol^{-1}), and (ii) the value of $K^{L}_{p,w}$ fixed at the value determined from the equilibrium isotherm data (black dashed curve; $K^{L}_{p,w}$ = 7075.3 m^3 mol^{-1}); the depletion profile (C) shows the values obtained from numerical computation, eqns (1-2b,3-5,7) (red curve). The maximal extent of bulk depletion is 93% in the kinetic sorption data, and from the fitted τ of 937.4 h the derived diffusion coefficient is $D_{X,p} = 6.67\times10^{-13}$ m^2 s^{-1}.

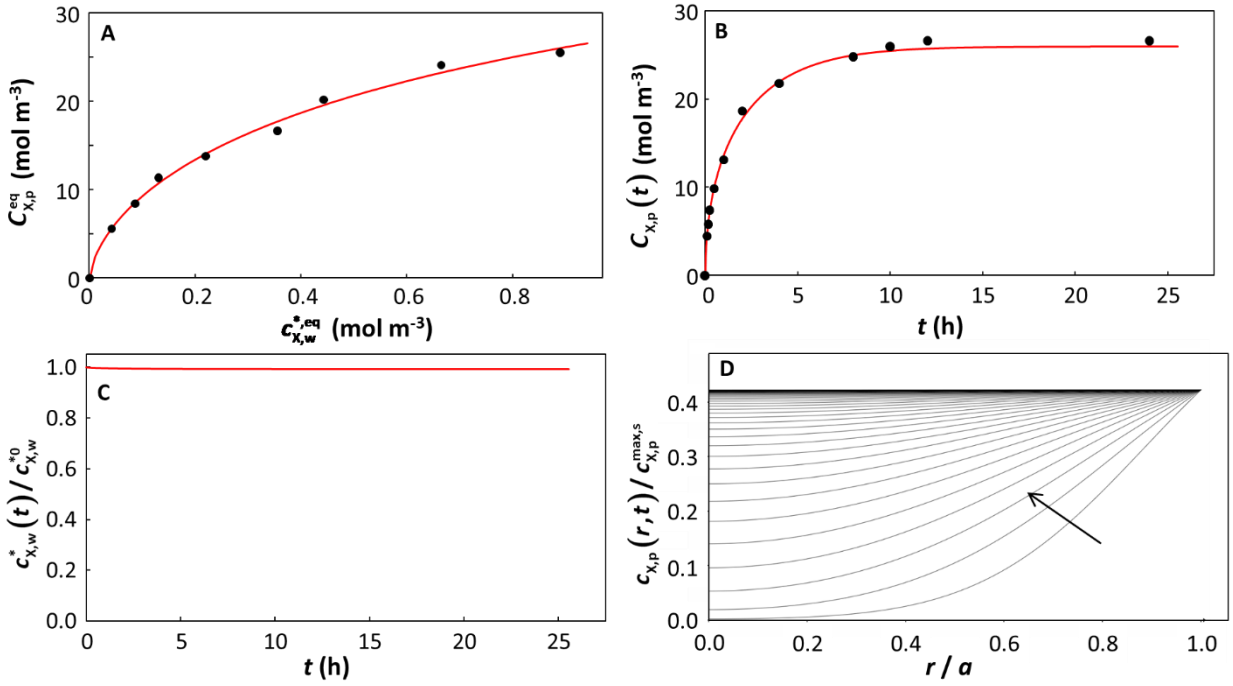

Fig. S8. Equilibrium and kinetic features of a system with low depletion of X in the bulk solution, Langmuir-Freundlich isotherm, $K^{LF}_{p,w}$ fixed during fitting of the kinetic data: sorption of Cd on polylactic acid particles (a = 1.5×10^{-5} m). The panels correspond to: **(A)** equilibrium sorption isotherm; **(B)** kinetic sorption curves; **(C)** corresponding solution depletion profile; and **(D)** temporal evolution of the normalized intraparticulate concentration profiles, with the direction of increasing time indicated by the arrow. In (D), the timescale between two plotted concentration profiles is $\Delta t =$ 1838 s, starting at $t =$ 1838 s. The situation at $t = 0$ (not shown) corresponds to plastic particles free of contaminants and to the initial bulk medium condition $c^{*}_{X,w}(t=0) = c^{*,0}_{X,w}$. The Langmuir-Freundlich isotherm best described the equilibrium data and τ was the only parameter that was optimized to fit the sorption curves (see **Table S1** for the pertaining parameters). The isotherm curve (A) shows the experimental data (black circles)[6] and the best fit obtained according to the Langmuir-Freundlich sorption isotherm (eqns (1-2c), red curve, adjusted parameter: $K^{LF}_{p,w}$); the kinetic sorption curve (B) shows the experimental data (black circles)[6] and the numerically computed values, eqns (1-2c,3-5,7-8) (red curve); the depletion profile (C) shows the values obtained from numerical computation, eqns (1-2c,3-5,7) (red curve). The maximal extent of bulk depletion is 1% in the kinetic sorption data, and from the fitted τ of 28.5 h the derived diffusion coefficient is $D_{X,p} = 2.19\times10^{-15}$ m^2 s^{-1}.

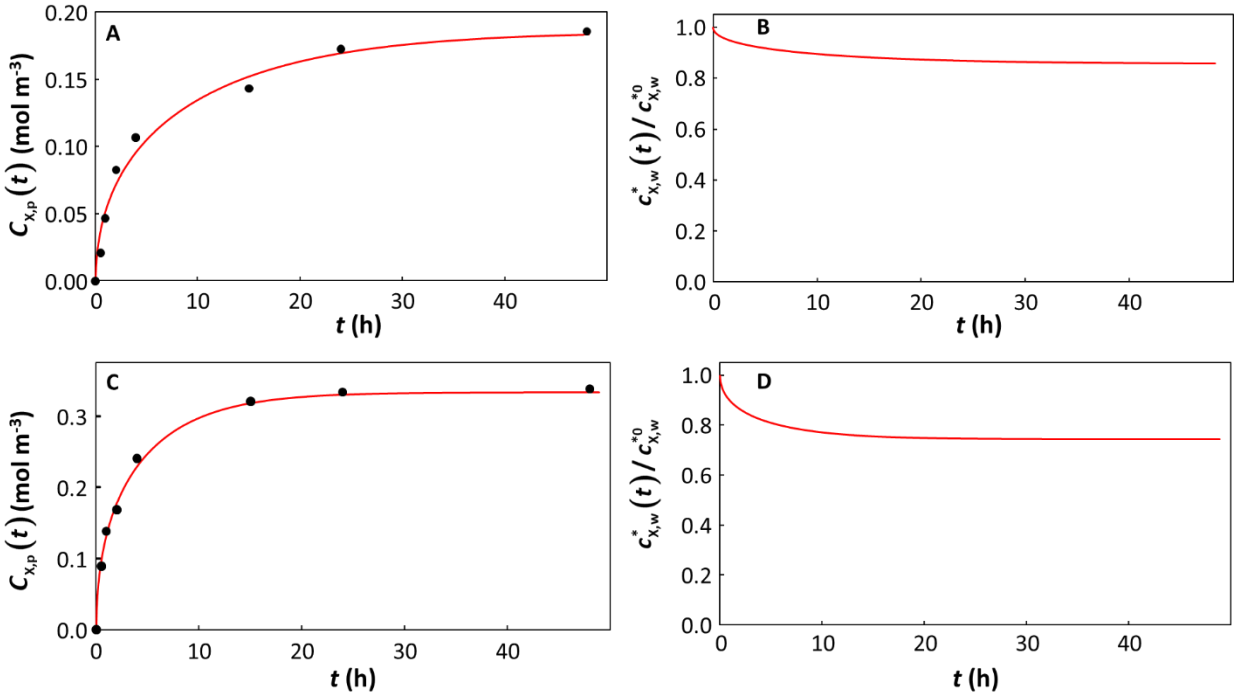

Fig. S9. Comparison of experimental and numerically computed sorption curves **(A,C)** and corresponding solution depletion profiles **(B,D)** for the sorption of benzophenone-3 on PS particles with a = 1.25×10^{-4} m (A,B, 14% bulk depletion) and 2.5×10^{-7} m (C,D, 25% bulk depletion) at the same particle volume fraction (6.7×10^{-4}). In both cases τ was the only parameter that was optimized to fit the sorption curves, and the Langmuir isotherm (eqns (1-2b)) best described the equilibrium data (see **Table S1** for the pertaining parameters). The sorption curves (A,C) show the experimental data (black circles)[7] and numerically computed values (eqns (1-2b,3-5,7-8), red curve); the depletion profiles (B,D) show the values obtained from numerical computation (eqns (1-2b,3-5,7), red curve). The difference in the extent of bulk depletion reflects the difference in Langmuir $c^{max,s}_{X,p}$ values (0.27 mol m^{-3} for a = 1.25×10^{-4} m; 0.42 mol m^{-3} for a = 2.5×10^{-7} m).

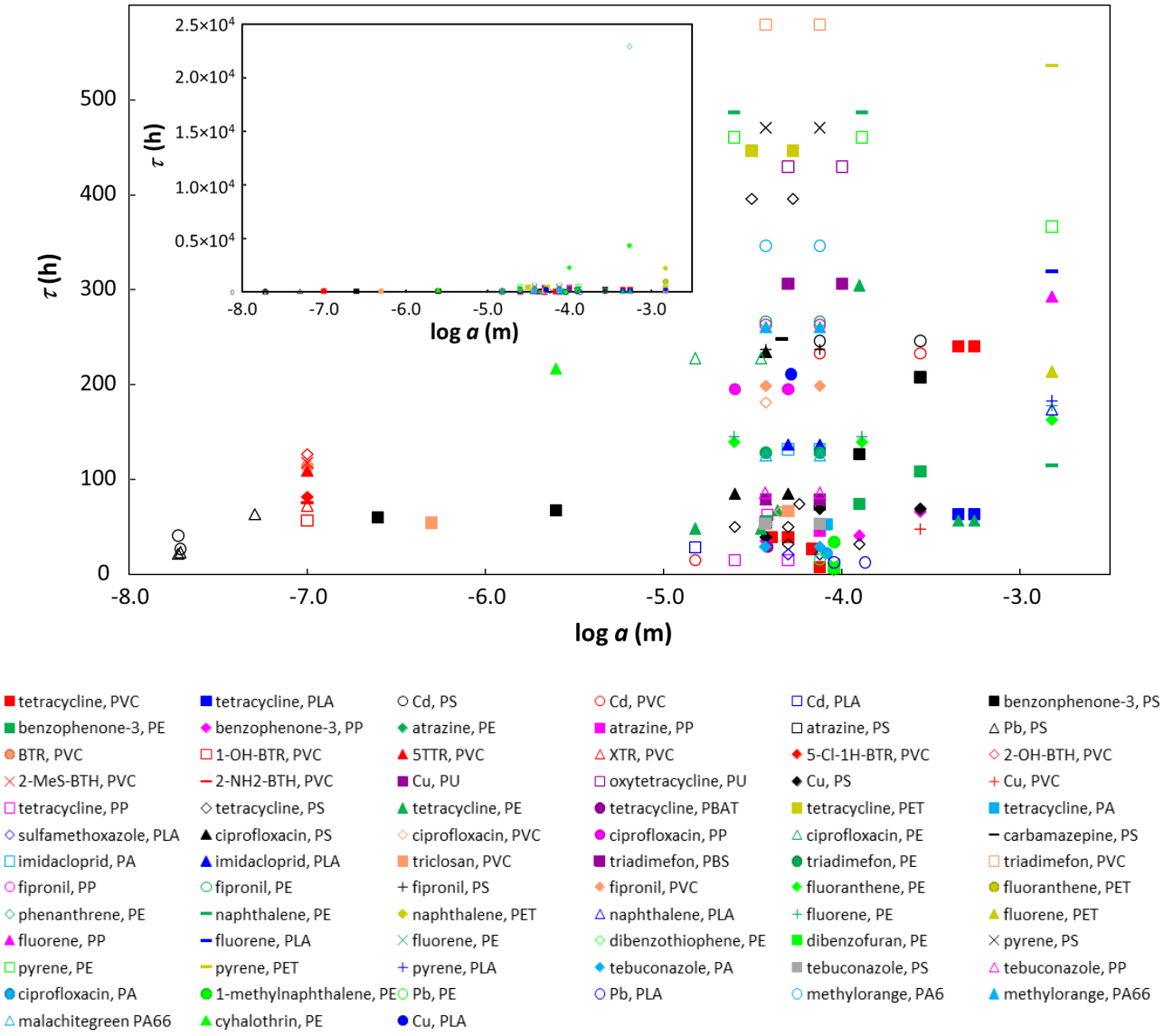

Fig. S10. The characteristic diffusion time, τ, as a function of the particle radius in logarithmic scale, log *a*. The inset at lower τ resolution shows the few data points with very high τ values. Symbols correspond to the analyzed data sets as specified in the legend. Abbreviations: PS = polystyrene; PVC = polyvinyl chloride; PLA = polylactic acid, PU = polyurethane; PP = polypropylene; PE = polyethylene; PBAT = polybutylene adipate terephthalate; PET = polyethylene terephthalate; PA = polyamide; PBS = polybutylene succinate; BTR = 1H-benzotriazole; 1-OH-BTR = 1-hydroxy-benzotriazole; 5TTR = 5-methyl-1H-benzotriazole; XTR = 5,6-dimethyl-1H-benzotriazole; 5-chloro-1H-BTR = 5-chloro-1H-benzotriazole; 2-OH-BTH = 2-hydroxy-benzothiazole; 2-MeS-BTH = 2-methylthio-benzothiazole; 2-NH2-BTH = 2-amino-benzothiazole.

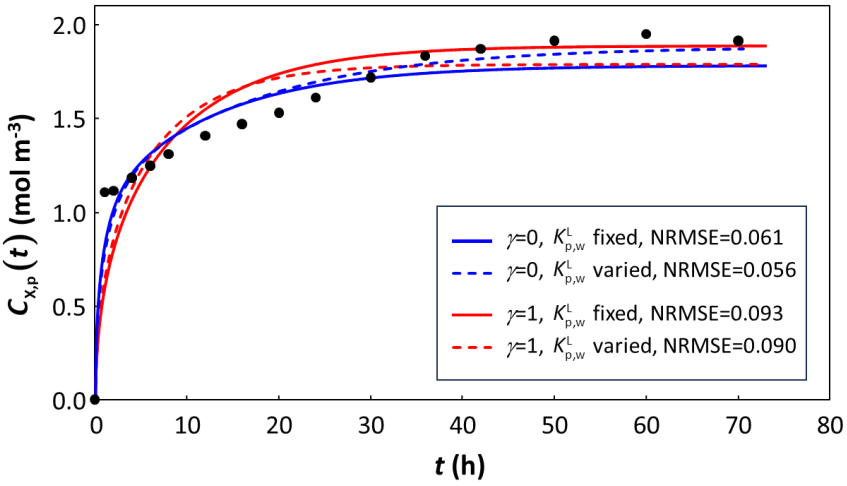

Fig. S11. Comparison of experimental and numerically computed sorption curves for the sorption of Cd(II) on PS particles with a =2.15-3.7×10^{-5} m, with an experimental volume fraction φ = 0.01. The Langmuir isotherm (eqns (1-2b)) best described the equilibrium data ($K^{L}_{p,w}$ = 0.47 m^3 mol^{-1}; $c^{max,s}_{X,p}$ = 9.69 mol m^{-3}). The various curves show the experimental data (black circles)[8] and numerically computed values (eqns (1-2b,3-5,7-8)) corresponding to optimization of only τ or both τ and $K^{L}_{p,w}$ to fit the sorption curve for both γ = 0 and γ = 1, as indicated in the legend. The value of $K^{L}_{p,w}$ optimized by the kinetic fitting was 0.51 m^3 mol^{-1} for γ = 0, and 0.44 m^3 mol^{-1} for γ = 1. All computations were performed using φ = 0.01; use of artificially lower φ values, with $K^{L}_{p,w}$ fixed or optimized during the kinetic fitting, did not further improve the fit to the data.

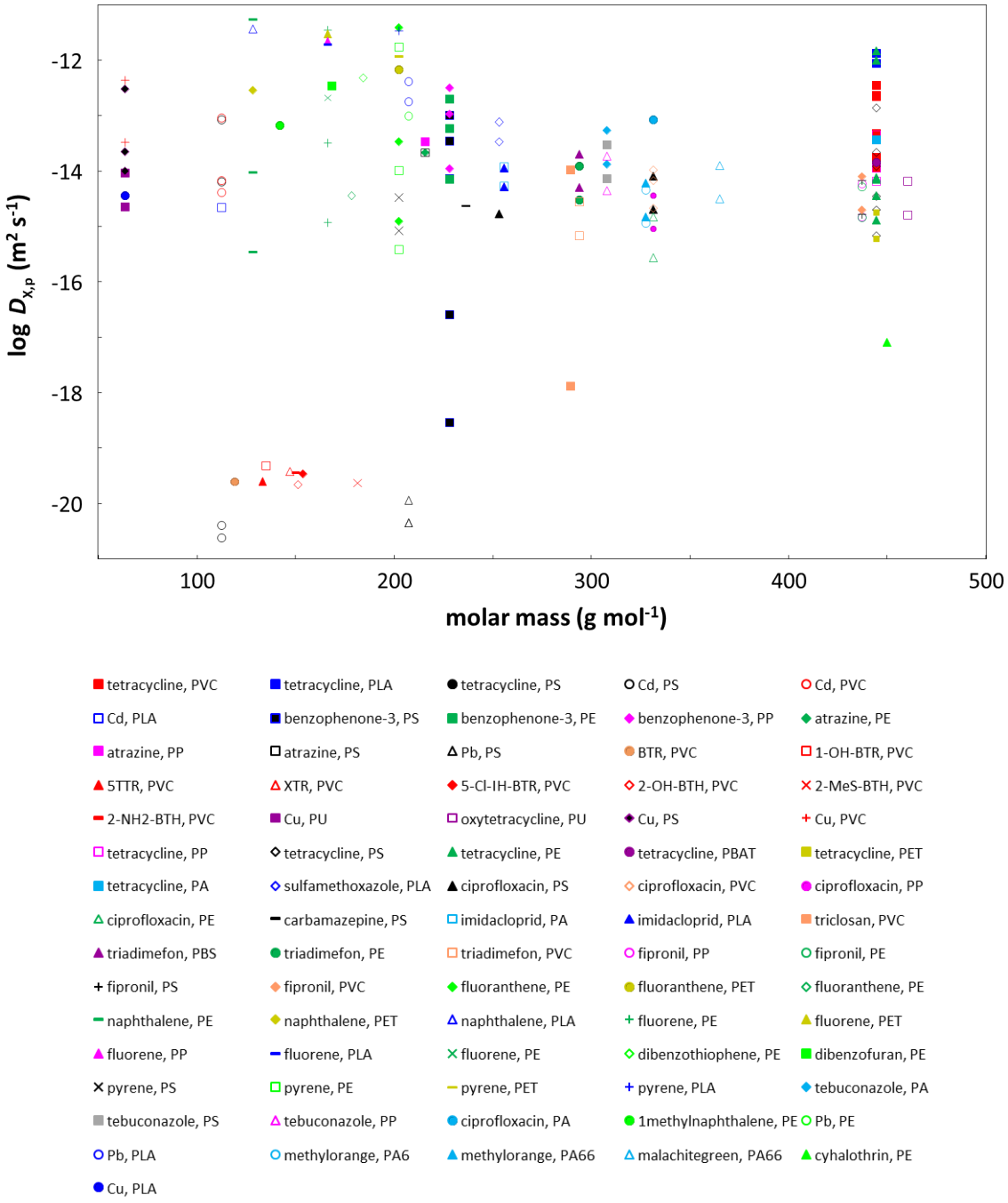

Fig. S12. Diffusion coefficient (in logarithmic scale) of the target molecule X in the polymer phase, log $D_{x,p}$, as a function of the molar mass of X. Symbols correspond to the analyzed data sets as specified in the legend. Abbreviations: PS = polystyrene; PVC = polyvinyl chloride; PLA = polylactic acid, PU = polyurethane; PP = polypropylene; PE = polyethylene; PBAT = polybutylene adipate terephthalate; PET = polyethylene terephthalate; PA = polyamide; PBS = polybutylene succinate; BTR = 1H-benzotriazole; 1-OH-BTR = 1-hydroxy-benzotriazole; 5TTR = 5-methyl-1H-benzotriazole; XTR = 5,6-dimethyl-1H-benzotriazole; 5-chloro-1H-BTR = 5-chloro-1H-benzotriazole; 2-OH-BTH = 2-hydroxy-benzothiazole; 2-MeS-BTH = 2-methylthio-benzothiazole; 2-NH2-BTH = 2-amino-benzothiazole.

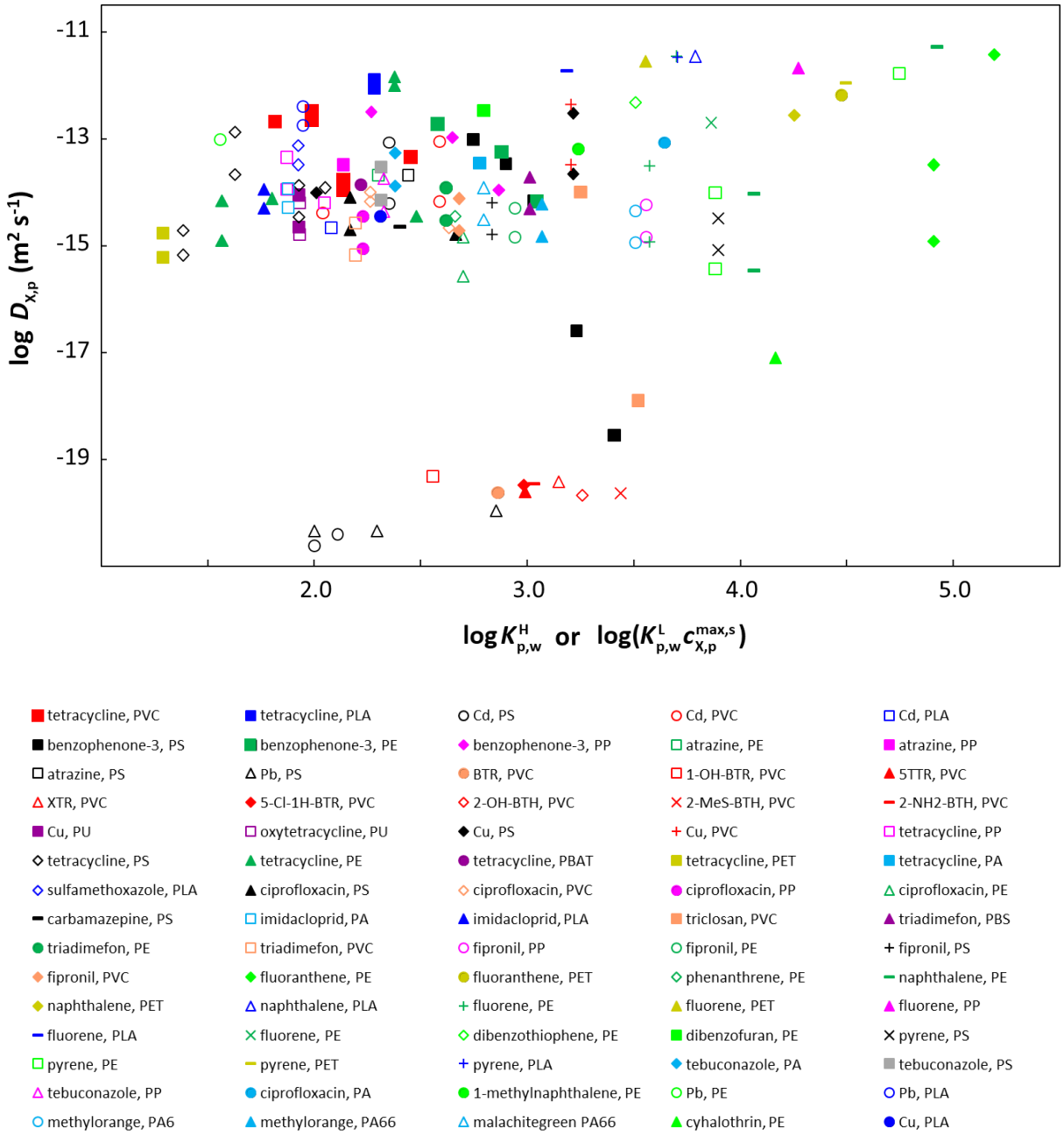

Fig. S13. Diffusion coefficient (in logarithmic scale) of the target molecule X in the polymer phase, $\log D_{X,p}$, as a function of the linearized (dimensionless) partition coefficient given in logarithmic scale, i.e. $\log K^H_{p,w}$ or $\log(K^L_{p,w}c^{max,s}_{X,p})$. Symbols correspond to the analyzed data sets as specified in the legend. Since it is not straightforward to linearize the Langmuir-Freundlich partition coefficient, for purposes of this plot, the few equilibrium data that are best described by the Langmuir-Freundlich isotherm were recalculated with a Langmuir isotherm, which typically also provided an adequate fit to the equilibrium data. Abbreviations: PS = polystyrene; PVC = polyvinyl chloride; PLA = polylactic acid, PU = polyurethane; PP = polypropylene; PE = polyethylene; PBAT = polybutylene adipate terephthalate; PET = polyethylene terephthalate; PA = polyamide; PBS = polybutylene succinate; BTR = 1H-benzotriazole; 1-OH-BTR = 1-hydroxy-benzotriazole; 5TTR = 5-methyl-1H-benzotriazole; XTR = 5,6-dimethyl-1H-benzotriazole; 5-chloro-1H-BTR = 5-chloro-1H-benzotriazole; 2-OH-BTH = 2-hydroxy-benzothiazole; 2-MeS-BTH = 2-methylthio-benzothiazole; 2-NH2-BTH = 2-amino-benzothiazole.

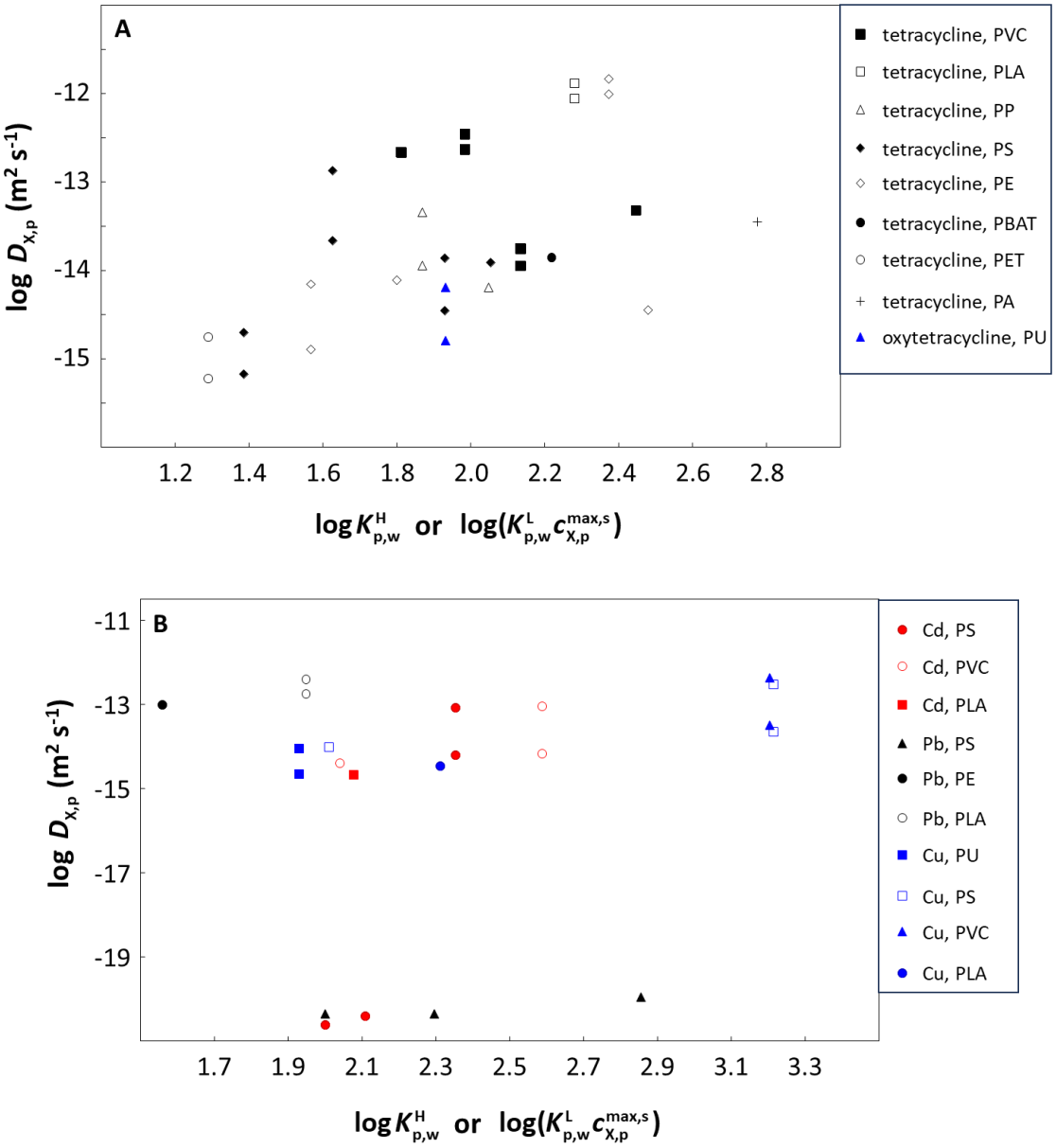

Fig. S14. Diffusion coefficient (in logarithmic scale) of the target contaminant **(A)** (oxy)tetracycline and **(B)** metal ions in the polymer phase, $\log D_{X,p}$, as a function of the linearized (dimensionless) partition coefficient given in logarithmic scale, i.e. $\log K^{H}_{p,w}$ or $\log(K^{L}_{p,w} c^{max,s}_{X,p})$. Symbols correspond to the analyzed data sets as specified in the legend. Since it is not straightforward to linearize the Langmuir-Freundlich partition coefficient, for purposes of this plot, the few equilibrium data that are best described by the Langmuir-Freundlich isotherm were recalculated with a Langmuir isotherm, which typically also provided an adequate fit to the equilibrium data. Abbreviations: PS = polystyrene; PVC = polyvinyl chloride; PLA = polylactic acid, PU = polyurethane; PP = polypropylene; PE = polyethylene; PBAT = polybutylene adipate terephthalate; PET = polyethylene terephthalate; PA = polyamide.

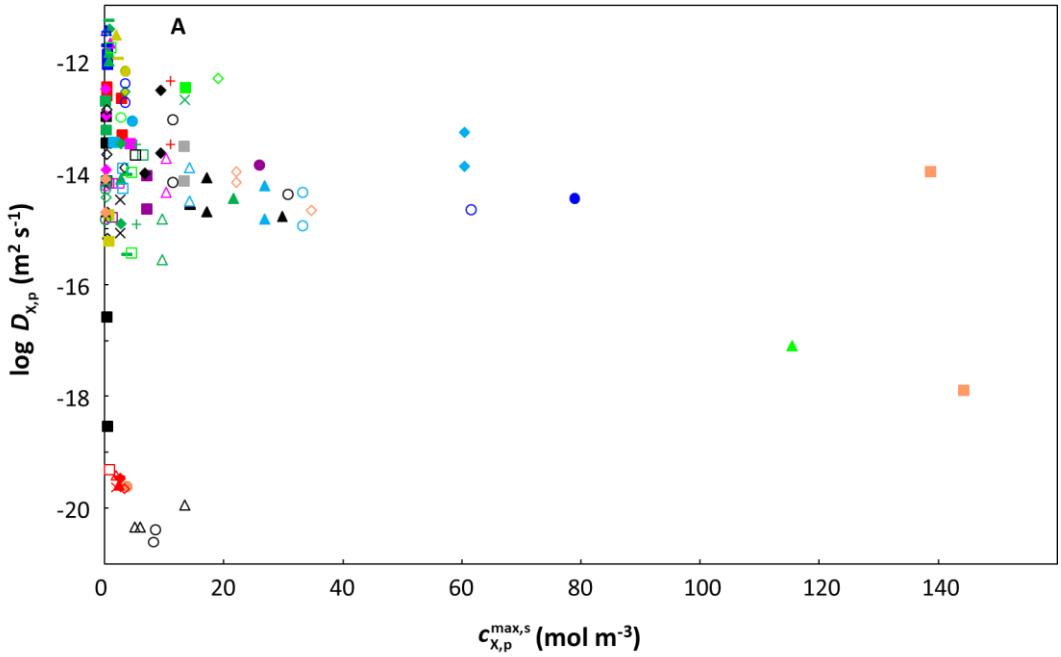
A
-12
-14
-16
-18
-20
log $D_{x,p}$ (m^2 s^{-1})
0
20
40
60
80
100
120
140
$c_{x,p}^{max,s}$ (mol m^{-3})

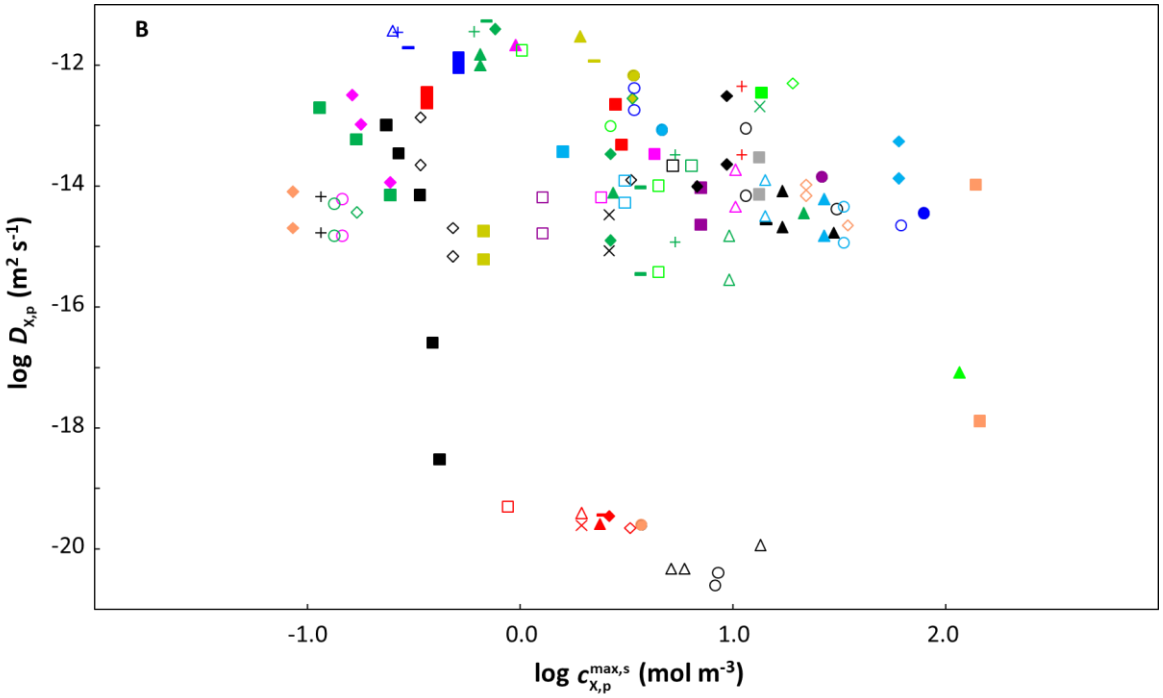
B
-12
-14
-16
-18
-20
log $D_{x,p}$ (m^2 s^{-1})
-1.0
0.0
1.0
2.0
log $c_{x,p}^{max,s}$ (mol m^{-3})

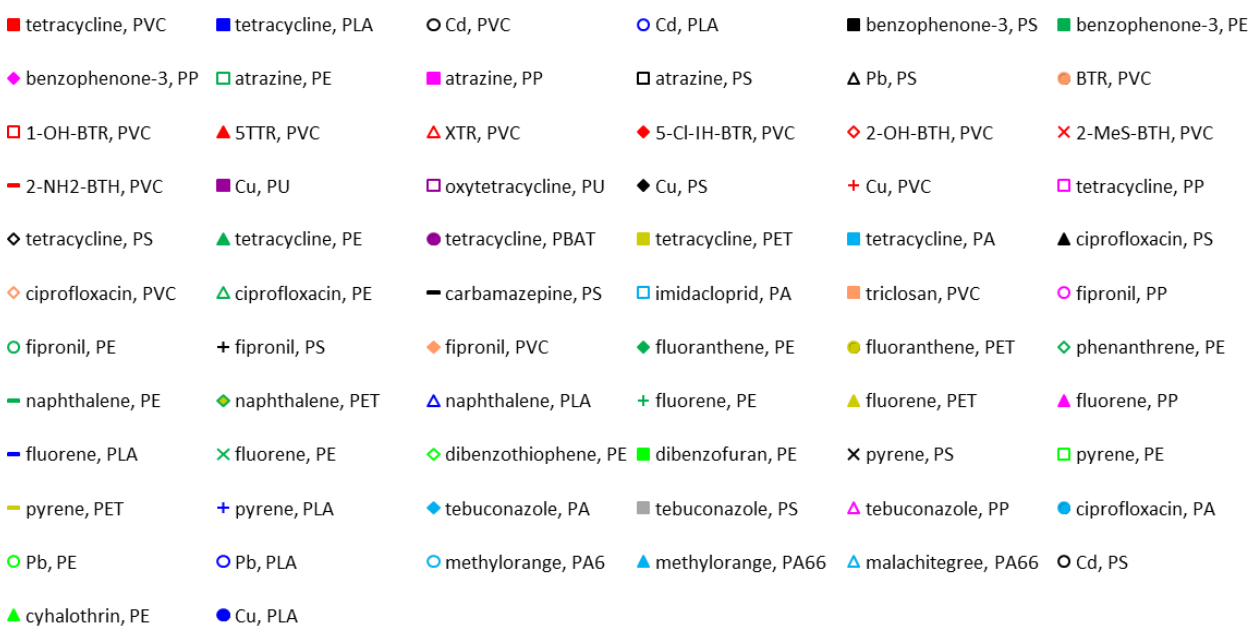

Fig. S15. Diffusion coefficient (in logarithmic scale) of the target molecule X in the polymer phase, log $D_{X,p}$, as a function of the maximum sorbed concentration at equilibrium, $c_{X,p}^{max,s}$ plotted in (**A**) log-linear and (**B**) log-log format. Symbols correspond to the analyzed data sets as detailed in the legend; the data correspond to those best described by a Langmuir or a Langmuir-Freundlich isotherm. Abbreviations: PS = polystyrene; PVC = polyvinyl chloride; PLA = polylactic acid, PU = polyurethane; PP = polypropylene; PE = polyethylene; PBAT = polybutylene adipate terephthalate; PET = polyethylene terephthalate; PA = polyamide; PBS = polybutylene succinate; BTR = 1H-benzotriazole; 1-OH-BTR = 1-hydroxy-benzotriazole; 5TTR = 5-methyl-1H-benzotriazole; XTR = 5,6-dimethyl-1H-benzotriazole; 5-chloro-1H-BTR = 5-chloro-1H-benzotriazole; 2-OH-BTH = 2-hydroxy-benzothiazole; 2-MeS-BTH = 2-methylthio-benzothiazole; 2-NH2-BTH = 2-amino-benzothiazole.

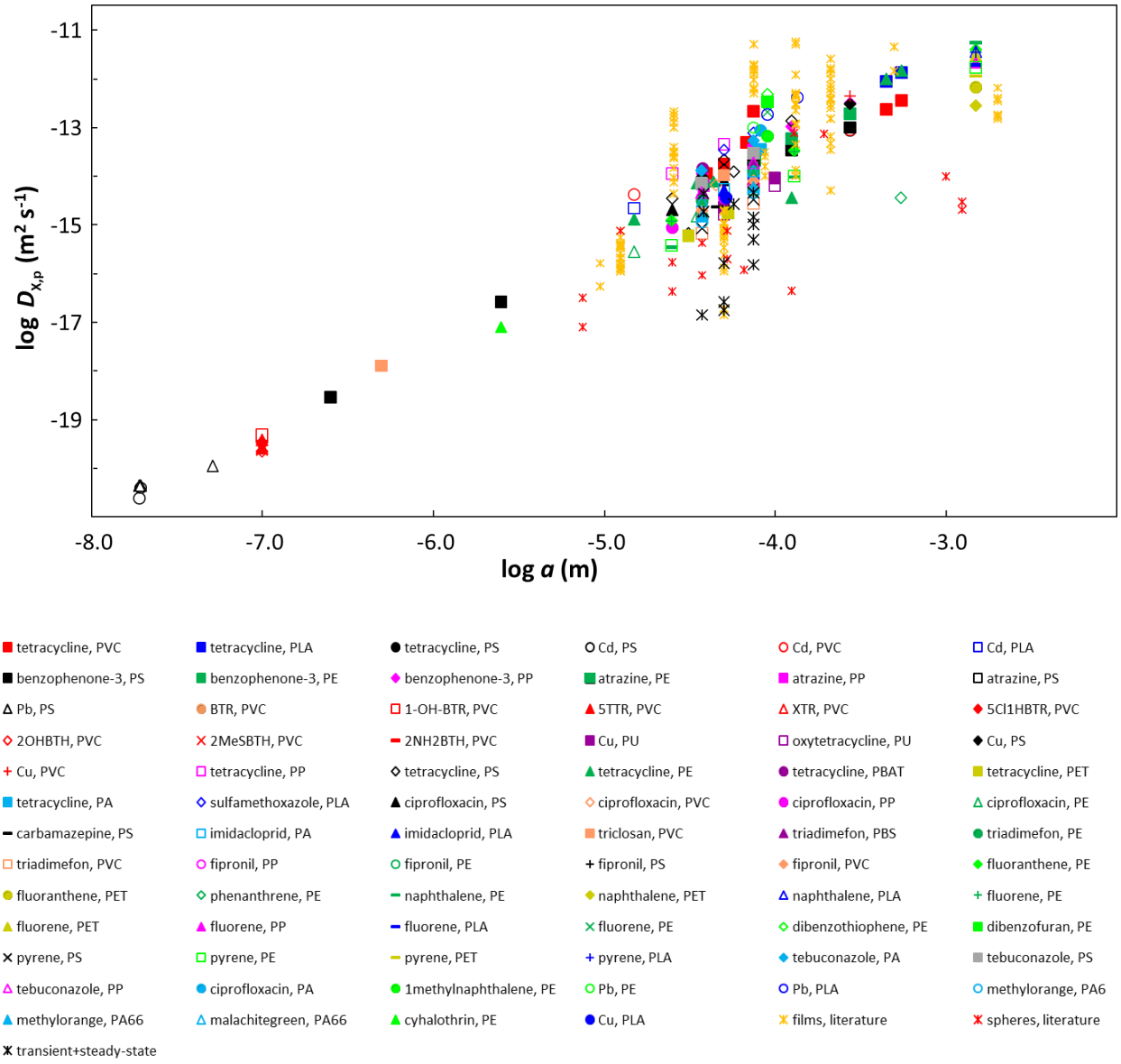

Fig. S16. Log-log plot of the intraparticulate diffusion coefficient, $D_{X,p}$, as a function of particle radius, a. Symbols correspond to the analyzed data sets as detailed in the legend. Included are literature reports of $D_{X,p}$ values (determined by various means) for thin films (yellow asterisks),[9-16] spheres (red asterisks),[16-19] and our previous coupled transient plus steady-state approach for spherical particles (black asterisks).[20] Abbreviations: PS = polystyrene; PVC = polyvinyl chloride; PLA = polylactic acid, PU = polyurethane; PP = polypropylene; PE = polyethylene; PBAT = polybutylene adipate terephthalate; PET = polyethylene terephthalate; PA = polyamide; PBS = polybutylene succinate; BTR = 1H-benzotriazole; 1-OH-BTR = 1-hydroxy-benzotriazole; 5TTR = 5-methyl-1H-benzotriazole; XTR = 5,6-dimethyl-1H-benzotriazole; 5-chloro-1H-BTR = 5-chloro-1H-benzotriazole; 2-OH-BTH = 2-hydroxy-benzothiazole; 2-MeS-BTH = 2-methylthio-benzothiazole; 2-NH2-BTH = 2-amino-benzothiazole.

Table S1. Polymers and compounds for which kinetic and equilibrium data are available. γ=1 in all cases, with one exception highlighted in yellow

polymer[a]	compound, X	particle radius, a (m)	particle volume fraction	% bulk depletion[b]	τ (h) [c]	$D_{X,p}$ (m^2 s^{-1}) [d]	NRMSE, kinetic fitting [c,e]	equilibrium isotherm [f]	Ref
PS	Cd	7.5×10^{-5} - 2.75×10^{-4}	1×10^{-3}	17.5	246.3 (196.4 – 296.2)	6.34×10^{-15} (75 µm) 8.50×10^{-14} (275 µm)	0.066	Henry $K^{H}_{p,w}$ =225.9 NRMSE=0.054	21
PS-NH_2	Cd	1.9×10^{-8}	1×10^{-4}	0.1	41.1 (30.8 – 51.4)	2.44×10^{-21}	0.063	Langmuir $c^{max,s}_{X,p}$ =8.22 $K^{L}_{p,w}$ =12.2 NRMSE=0.033	22
PS-SO_3H	Cd	1.95×10^{-8}	1×10^{-4}	0.2	26.6 (17.7 – 35.4)	3.98×10^{-21}	0.074	Langmuir $c^{max,s}_{X,p}$ =8.53 $K^{L}_{p,w}$ =15.1 NRMSE = 0.030	22
PVC	Cd	7.5×10^{-5} - 2.75×10^{-4}	1×10^{-3}	35.4	232.5 (162.7 – 302.3) γ=0	6.72×10^{-15} (75 µm) 9.03×10^{-14} (275 µm)	0.079	Langmuir $c^{max,s}_{X,p}$ =11.5 $K^{L}_{p,w}$ =33.8 NRMSE=0.060	21
PLA	Cd	1.5×10^{-5}	2×10^{-4}	0.6	28.5 (26.0 – 31.1)	2.19×10^{-15}	0.018	LF, p_{LF} = 1.55 $c^{max,s}_{X,p}$ =61.53 $K^{LF}_{p,w}$ =0.7 NRMSE=0.022	6
PVC	Cd	1.5×10^{-5}	2×10^{-4}	0.4	15.2 (11.5 – 18.9-	4.11×10^{-15}	0.049	LF, p_{LF} = 1.637 $c^{max,s}_{X,p}$ =30.74 $K^{LF}_{p,w}$ =1.4 NRMSE=0.025	6
PU	Cu	5×10^{-5} - 1×10^{-4}	3.33×10^{-3}	9.0	306.6 (190.4 – 422.9)	2.27×10^{-15} (50 µm) 9.06×10^{-15} (100 µm)	0.061	Langmuir $c^{max,s}_{X,p}$ =7.09 $K^{L}_{p,w}$ =12.0 NRMSE=0.036	23

polymer[a]	compound, X	particle radius, a (m)	particle volume fraction	% bulk depletion[b]	τ (h) [c]	$D_{X,p}$ (m^2 s^{-1}) [d]	NRMSE, kinetic fitting [c,e]	equilibrium isotherm [f]	Ref
PS	Cu	7.5×10^{-5} - 2.75×10^{-4}	1×10^{-3}	36.7	69.2 (57.1 – 81.2)	2.26×10^{-14} (75 µm) 3.04×10^{-13} (275 µm)	0.044	Langmuir $c_{X,p}^{max,s}$ =9.37; $K_{p,w}^{LF}$ 175.1 NRMSE=0.062	21
PS	Cu	3.726×10^{-5}	1×10^{-3}	3.3	39.1 (30.1 – 48.1)	9.86×10^{-15}	0.031 [$K_{p,w}^{L}$ varied: 20.1 (16.7 – 23.5)]	Langmuir $c_{X,p}^{max,s}$ = 6.79 $K_{p,w}^{L}$ =15.1 NRMSE=0.056	24
PLA	Cu	5.1815×10^{-5}	1×10^{-3}	12.4	211.5 (173.5 – 249.4)	3.53×10^{-15}	0.043	Langmuir $c_{X,p}^{max,s}$ =78.90 $K_{p,w}^{L}$ =2.6 NRMSE=0.031	24
PVC	Cu	7.5×10^{-5} - 2.75×10^{-4}	1×10^{-3}	32.5	47.8 (33.1 – 62.5)	3.27×10^{-14} (75 µm) 4.40×10^{-13} (275 µm)	0.051 [$K_{p,w}^{L}$ varied: 81.6 (70.7 -92.4)]	Langmuir $c_{X,p}^{max,s}$ =11.03 $K_{p,w}^{LF}$ =145.6 NRMSE=0.076	21
PS	Pb	5.105×10^{-8}	1.25×10^{-3}	32.4	63.8 (28.7 – 99.0)	1.13×10^{-20}	0.096	Langmuir $c_{X,p}^{max,s}$ = 13.46 $K_{p,w}^{L}$ =53.2 NRMSE=0.051	25
PS-NH_2	Pb	1.9×10^{-8}	1×10^{-4}	0.2	22.1 (17.4 – 26.9)	4.53×10^{-21}	0.045	Langmuir $c_{X,p}^{max,s}$ = 5.12 $K_{p,w}^{L}$ =19.6 NRMSE=0.030	22
PS-SO_3H	Pb	1.95×10^{-8}	1×10^{-4}	0.2	23.3 (16.4 – 30.1)	4.54×10^{-21}	0.063	Langmuir $c_{X,p}^{max,s}$ =5.91 $K_{p,w}^{L}$ =33.5 NRMSE=0.027	22

polymer[a]	compound, X	particle radius, a (m)	particle volume fraction	% bulk depletion[b]	τ (h) [c]	$D_{X,p}$ (m^2 s^{-1}) [d]	NRMSE, kinetic fitting [c,e]	equilibrium isotherm [f]	Ref
PE	Pb	7.5×10^{-5}	5×10^{-3}	9.6	15.9	9.85×10^{-14}	0.036 [$K^{L}_{p,w}$ varied: 16.4 (14.6 – 18.1)]	Langmuir $c^{max,s}_{X,p}$ =2.67 $K^{L}_{p,w}$ =13.6 NRMSE=0.039	26
PLA	Pb	9×10^{-5} – 1.35×10^{-4}	5×10^{-3}	15.6	12.5	1.80×10^{-13} (90 µm) 4.05×10^{-13} (135 µm)	0.032 [$K^{L}_{p,w}$ varied: 31.2 (27.0 – 35.5)]	Langmuir $c^{max,s}_{X,p}$ =3.42 $K^{L}_{p,w}$ =26.0 NRMSE=0.014	26
PU	oxytetracycline	5×10^{-5} - 1×10^{-4}	3.333×10^{-3}	10.0	429.5 (375.0 – 484.1)	1.62×10^{-15} (50 µm) 6.47×10^{-15} (100 µm)	0.028	Langmuir $c^{max,s}_{X,p}$ =1.27 $K^{L}_{p,w}$ =67.2 NRMSE=0.049	23
PP	tetracycline	3.83×10^{-5}	1×10^{-3}	5.0	63.0 (22.2 – 103.9)	6.47×10^{-15}	0.059 [$K^{L}_{p,w}$ varied: 46.8 (29.5 – 64.0)]	Langmuir $c^{max,s}_{X,p}$ = 2.40 $K^{L}_{p,w}$ =35.6 NRMSE=0.022	27
PS	tetracycline	5×10^{-5} – 1.25×10^{-4}	6.667×10^{-3}	4.3	32.1 (17.1 – 47.1)	2.16×10^{-14} (50 µm) 1.35×10^{-13} (125 µm)	0.087	Langmuir $c^{max,s}_{X,p}$ =0.34 $K^{L}_{p,w}$ =124.3 NRMSE=0.059	28
PS	tetracycline	3.1×10^{-5} – 5.3×10^{-5}	5×10^{-3}	3.4	395.8 (285.3 – 506.3)	6.75×10^{-16} (31 µm) 1.97×10^{-15} (53 µm)	0.072	Langmuir $c^{max,s}_{X,p}$ =0.48 $K^{L}_{p,w}$ =50.6 NRMSE=0.080	28
PS	tetracycline	5.73×10^{-5}	1×10^{-3}	7.7	74.6 (34.0 – 115.3)	1.22×10^{-14}	0.043 [$K^{L}_{p,w}$ varied: 63.7 (39.1 – 88.2)]	Langmuir $c^{max,s}_{X,p}$ = 3.33 $K^{L}_{p,w}$ =34.0 NRMSE=0.025	27

polymer[a]	compound, X	particle radius, a (m)	particle volume fraction	% bulk depletion[b]	τ (h) [c]	$D_{X,p}$ (m^2 s^{-1}) [d]	NRMSE, kinetic fitting [c,e]	equilibrium isotherm [f]	Ref
PE	tetracycline	4.34×10^{-5}	1×10^{-3}	4.1	67.4 (50.9 – 83.9)	7.76×10^{-15}	0.072	Langmuir $c_{X,p}^{max,s}$ =2.74 $K_{p,w}^{L}$ =23.1 NRMSE=0.020	27
PE	tetracycline	1.25×10^{-4}	5×10^{-4}	11.7	304.7 (150.4 – 459.0)	3.56×10^{-15}	0.058 [$K_{p,w}^{L}$ varied: 14.0 (12.5 – 15.5)]	Langmuir $c_{X,p}^{max,s}$ =21.57 $K_{p,w}^{L}$ =4.6 NRMSE=0.028	29
PBAT	tetracycline	3.82×10^{-5}	1×10^{-3}	7.9	29.1 (25.2 – 32.9)	1.40×10^{-14}	0.030	LF, p_{LF} = 2.60 $c_{X,p}^{max,s}$ =26.0 $K_{p,w}^{LF}$ =0.054 NRMSE=0.009	27
PET	tetracycline	3.1×10^{-5} – 5.3×10^{-5}	5×10^{-3}	3.7	446.1 (341.2 – 551.0)	5.98×10^{-16} (31 µm) 1.75×10^{-15} (53 µm)	0.065	Langmuir $c_{X,p}^{max,s}$ =0.67 $K_{p,w}^{L}$ =29.1 NRMSE=0.055	30
PA	tetracycline	8.235×10^{-5}	2×10^{-3}	23.5	52.4 (41.3 – 63.6)	3.59×10^{-14}	0.038	Langmuir $c_{X,p}^{max,s}$ =1.58 $K_{p,w}^{L}$ =377.0 NRMSE=0.060	31
PVC	tetracycline	6.795×10^{-5}	2×10^{-3}	24.8	27.0 (16.9-37.1)	4.75×10^{-14}	0.044 [$K_{p,w}^{L}$ varied: 93.3 (81.2-105.4)]	Langmuir $c_{X,p}^{max,s}$ =3.01 $K_{p,w}^{L}$ =277.7 NRMSE=0.067	31
PVC	tetracycline	7.5×10^{-5}	1×10^{-3}	4.2	7.2 (4.1 – 10.3)	2.17×10^{-13}	0.065 [$K_{p,w}^{L}$ varied: 23.1 (20.6-25.7)]	Langmuir $c_{X,p}^{max,s}$ =2.81 $K_{p,w}^{L}$ =32.7 NRMSE=0.032	32

polymer[a]	compound, X	particle radius, a (m)	particle volume fraction	% bulk depletion[b]	τ (h) [c]	$D_{X,p}$ (m^2 s^{-1}) [d]	NRMSE, kinetic fitting [c,e]	equilibrium isotherm [f]	Ref
PVC	tetracycline	4.5×10^{-4} – 5.5×10^{-4}	5×10^{-3}	11.6	240.4 (146.1 – 334.8)	2.34×10^{-13} (450 µm) 3.50×10^{-13} (550 µm)	0.045 [$K^{L}_{p,w}$ varied: 265.7 (166.0-365.4)]	Langmuir $c^{max,s}_{X,p}$ =0.36 $K^{L}_{p,w}$ =82.9 NRMSE=0.037	33
PLA	tetracycline	4.5×10^{-4} – 5.5×10^{-4}	5×10^{-3}	17.7	63.5 (45.7 – 81.3)	8.86×10^{-13} (450 µm) 1.32×10^{-12} (550 µm)	0.040 [$K^{L}_{p,w}$ varied: 375.0 (285.4-464.6)]	Langmuir $c^{max,s}_{X,p}$ =0.51 $K^{L}_{p,w}$ =126.5 NRMSE=0.022	33
PE	tetracycline	4.5×10^{-4} – 5.5×10^{-4}	5×10^{-3}	22.1	57.2 (35.7 – 78.8)	9.83×10^{-13} (450 µm) 1.47×10^{-12} (550 µm)	0.054 [$K^{L}_{p,w}$ varied: 365.0 (255.4-474.5)]	Langmuir $c^{max,s}_{X,p}$ = 0.65 $K^{L}_{p,w}$ =154.9 NRMSE=0.011	33
PVC	tetracycline	4×10^{-5} - 5×10^{-5}	1×10^{-3}	9.5	39.4 (30.1 – 48.6)	1.13×10^{-14} (40 µm) 1.76×10^{-14} (50 µm)	0.031 [$K^{H}_{p,w}$ varied: 104.8 (100.3-109.4)]	Henry $K^{H}_{p,w}$ =136.4 NRMSE=0.093	2
PP	tetracycline	2.5×10^{-5} – 5×10^{-5}	1×10^{-3}	6.9	15.4 (12.1 – 18.7)	1.13×10^{-14} (25 µm) 4.52×10^{-14} (50 µm)	0.030 [$K^{H}_{p,w}$ varied: 74.2 (71.9-76.6)	Henry $K^{H}_{p,w}$ =98.5 NRMSE=0.125	2
PS	tetracycline	2.5×10^{-5} – 5×10^{-5}	1×10^{-3}	7.9	49.9 (30.7 – 69.2)	3.48×10^{-15} (25 µm) 1.39×10^{-14} (50 µm)	0.057 [$K^{H}_{p,w}$ varied: 85.2 (78.2-92.2)	Henry $K^{H}_{p,w}$ =108.2 NRMSE=0.081	2
PE	tetracycline	1.5×10^{-5} – 3.5×10^{-5}	1×10^{-3}	3.5	48.5 (20.8 – 76.2)	1.29×10^{-15} (15 µm) 7.01×10^{-15} (35 µm)	0.079 [$K^{H}_{p,w}$ varied: 36.7 (32.3-41.2)	Henry $K^{H}_{p,w}$ =99.1 NRMSE=0.127	2
PLA	sulfamethoxazole	5×10^{-5} – 7.5×10^{-5}	2×10^{-3}	14.4	20.7 (15.6 – 25.7)	3.36×10^{-14} (50 µm) 7.56×10^{-14} (75 µm)	0.025 [$K^{H}_{p,w}$ varied: 84.0 (79.9 – 88.2)]	Henry $K^{H}_{p,w}$ =66.5 NRMSE=0.030	34
PS	ciprofloxacin	3.75×10^{-5}	4×10^{-4}	10.9	234.3 (152.6 – 315.9)	1.67×10^{-15}	0.096	Langmuir $c^{max,s}_{X,p}$ =29.81 $K^{L}_{p,w}$ =15.5 NRMSE=0.089	35

polymer[a]	compound, X	particle radius, a (m)	particle volume fraction	% bulk depletion[b]	τ (h) [c]	$D_{X,p}$ (m^2 s^{-1}) [d]	NRMSE, kinetic fitting [c,e]	equilibrium isotherm [f]	Ref
PVC	ciprofloxacin	3.75×10^{-5}	4×10^{-4}	11.1	181.1 (118.8 – 243.4)	2.16×10^{-15}	0.087	Langmuir $c_{X,p}^{max,s}$ =34.75 $K_{p,w}^{L}$ =12.3 NRMSE=0.062	35
PA	ciprofloxacin	8.235×10^{-5}	2×10^{-3}	69.1	22.2 (14.8 – 29.5)	8.50×10^{-14}	0.040 [$K_{p,w}^{L}$ varied: 952.2 (628.8 – 1275.5)]	Langmuir $c_{X,p}^{max,s}$ =4.62 $K_{p,w}^{L}$ =165.6 NRMSE=0.073	31
PVC	ciprofloxacin	4×10^{-5}- 5×10^{-5}	1×10^{-3}	13.1	66.3 (40.8 – 91.8)	6.70×10^{-15} (40 µm) 1.05×10^{-14} (50 µm)	0.052 [$K_{p,w}^{L}$ varied: 8.3 (7.5 – 9.2)]	Langmuir $c_{X,p}^{max,s}$ =22.04 $K_{p,w}^{L}$ =11.1 NRMSE=0.078	2
PP	ciprofloxacin	2.5×10^{-5} – 5×10^{-5}	1×10^{-3}	15.6	195.6 (124.8 – 266.3)	8.88×10^{-16} (25 µm) 3.55×10^{-15} (50 µm)	0.079	Henry $K_{p,w}^{H}$ =169.5 NRMSE=0.074	2
PS	ciprofloxacin	2.5×10^{-5} – 5×10^{-5}	1×10^{-3}	10.7	85.1 (68.1 – 102.1)	2.04×10^{-15} (25 µm) 8.16×10^{-15} (50 µm)	0.026 [$K_{p,w}^{L}$ varied: 8.6 (8.1 – 9.1)]	Langmuir $c_{X,p}^{max,s}$ =17.06 $K_{p,w}^{L}$ =16.2 NRMSE=0.041	2
PE	ciprofloxacin	1.5×10^{-5} – 3.5×10^{-5}	1×10^{-3}	18.8	228.2 (138.7 – 317.7)	2.74×10^{-16} (15 µm) 1.49×10^{-15} (35 µm)	0.089	Langmuir $c_{X,p}^{max,s}$ =9.57 $K_{p,w}^{L}$ =52.4 NRMSE=0.021	2
PE	atrazine	7.5×10^{-5}	4×10^{-4}	4.4	73.8 (48.2 – 99.3)	2.12×10^{-14}	0.029 [$K_{p,w}^{L}$ varied: 31.6 (26.4 – 36.7)]	Langmuir $c_{X,p}^{max,s}$ =6.3 $K_{p,w}^{L}$ =25.3 NRMSE=0.027	36

polymer[a]	compound, X	particle radius, a (m)	particle volume fraction	% bulk depletion[b]	τ (h) [c]	$D_{X,p}$ (m^2 s^{-1}) [d]	NRMSE, kinetic fitting [c,e]	equilibrium isotherm [f]	Ref
PP	atrazine	7.5×10^{-5}	4×10^{-4}	3.4	46.3 (35.4 – 57.2)	3.37×10^{-14}	0.043	Langmuir $c_{X,p}^{max,s}$ =4.28 $K_{p,w}^{L}$ =31.9 NRMSE=0.020	36
PS	atrazine	7.5×10^{-5}	4×10^{-4}	4.8	73.7 (33.0 – 114.4)	2.12×10^{-14}	0.046 [$K_{p,w}^{L}$ varied: 52.7 (35.2 – 70.3)]	Langmuir $c_{X,p}^{max,s}$ =5.22 $K_{p,w}^{L}$ =36.9 NRMSE=0.034	36
PS	carbamazepine	4.6×10^{-5}	4×10^{-4}	5.1	248.9 (169.1 – 328.8)	2.36×10^{-15}	0.026 [$K_{p,w}^{L}$ varied: 17.6 (14.7 – 20.5)]	Langmuir $c_{X,p}^{max,s}$ =14.32 $K_{p,w}^{L}$ =19.5 NRMSE=0.029	4
PA	imidacloprid	5×10^{-5} – 7.5×10^{-5}	3×10^{-3}	16.1	131.7 (108.2 – 155.2)	5.27×10^{-15} (50 µm) 1.19×10^{-14} (75 µm)	0.049	Langmuir $c_{X,p}^{max,s}$ =3.10 $K_{p,w}^{L}$ =24.4 NRMSE=0.020	37
PLA	imidacloprid	5×10^{-5}– 7.5×10^{-5}	3×10^{-3}	14.5	136.6 (69.2 – 204.1)	5.08×10^{-15} (50 µm) 1.14×10^{-14} (75 µm)	0.057 [$K_{p,w}^{H}$ varied: 57.8 (50.6 – 64.9)]	Henry $K_{p,w}^{H}$ = 50.3 NRMSE=0.040	37
PVC	triclosan	5×10^{-7}	4×10^{-4}	48.6	54.3 (41.5 – 67.0)	1.28×10^{-18}	0.024 [$K_{p,w}^{L}$ varied: 23.2 (21.3 – 25.0)]	Langmuir $c_{X,p}^{max,s}$ =144.34 $K_{p,w}^{L}$ =18.1 NRMSE=0.083	38
PVC	triclosan	5×10^{-5}	4×10^{-4}	35.5	66.6 (52.6 – 80.6)	1.04×10^{-14}	0.044	Langmuir $c_{X,p}^{max,s}$ =138.70 $K_{p,w}^{L}$ =12.8 NRMSE=0.087	38
PBS	triadimefon	3.75×10^{-5} – 7.5×10^{-5}	1×10^{-3}	50.7	79.0 (64.8 – 93.2)	4.94×10^{-15} (37.5 µm) 1.98×10^{-14} (75 µm)	0.022	Henry $K_{p,w}^{H}$ =1026.6 NRMSE=0.034	1

polymer[a]	compound, X	particle radius, a (m)	particle volume fraction	% bulk depletion[b]	τ (h) [c]	$D_{X,p}$ (m^2 s^{-1}) [d]	NRMSE, kinetic fitting [c,e]	equilibrium isotherm [f]	Ref
PE	triadimefon	3.75×10^{-5} – 7.5×10^{-5}	1×10^{-3}	29.4	128.9 (81.6 – 176.2)	3.03×10^{-15} (37.5 µm) 1.21×10^{-14} (75 µm)	0.035 [$K^{H}_{p,w}$ varied: 416.2 (377.3 – 455.1)]	Henry $K^{H}_{p,w}$ =222.0 NRMSE=0.028	1
PVC	triadimefon	3.75×10^{-5} – 7.5×10^{-5}	1×10^{-3}	12.8	578.6 (448.4 – 708.7)	6.75×10^{-16} (37.5 µm) 2.70×10^{-15} (75 µm)	0.043	Henry $K^{H}_{p,w}$ =156.4 NRMSE=0.035	1
PP	fipronil	3.75×10^{-5} – 7.5×10^{-5}	1×10^{-3}	28.1	262.8 (210.0 – 315.5)	1.49×10^{-15} (37.5 µm) 5.95×10^{-15} (75 µm)	0.025 [$K^{L}_{p,w}$ varied: 2.49×10^{4} (1.25×10^{4} – 3.73×10^{4})]	Langmuir $c^{max,s}_{X,p}$ =0.15 $K^{L}_{p,w}$ =1.102×10^{4} NRMSE=0.017	39
PE	fipronil	3.75×10^{-5} – 7.5×10^{-5}	1×10^{-3}	20.4	266.2 (204.2 – 328.2)	1.47×10^{-15} (37.5 µm) 5.09×10^{-15} (75 µm)	0.021 [$K^{L}_{p,w}$ varied and 8th data point omitted: 6553.8 (5100.4 – 8005.2)]	Langmuir $c^{max,s}_{X,p}$ =0.13 $K^{L}_{p,w}$ =4921.9 NRMSE=0.011	39
PS	fipronil	3.75×10^{-5} – 7.5×10^{-5}	1×10^{-3}	17.4	236.6 (206.2 – 267.0)	1.65×10^{-15} (37.5 µm) 6.60×10^{-15} (75 µm)	0.028	Langmuir $c^{max,s}_{X,p}$ =0.12 $K^{L}_{p,w}$ =5865.5 NRMSE=0.016	39
PVC	fipronil	3.75×10^{-5} – 7.5×10^{-5}	1×10^{-3}	12.8	198.7 (164.4 – 233.0)	1.97×10^{-15} (37.5 µm) 7.86×10^{-15} (75 µm)	0.036	Langmuir $c^{max,s}_{X,p}$ =0.085 $K^{L}_{p,w}$ =5634.4 NRMSE=0.010	39
PBS	fipronil	3.75×10^{-5} – 7.5×10^{-5}	1×10^{-3}	39.3	101.4 (87.3 – 115.4)	3.85×10^{-15} (37.5 µm) 1.54×10^{-14} (75 µm)	0.016 [$K^{L}_{p,w}$ varied: 504.8 (481.6 – 528.1)]	Langmuir $c^{max,s}_{X,p}$ =1.46 $K^{L}_{p,w}$ =3251.4 NRMSE=0.009	39

polymer[a]	compound, X	particle radius, a (m)	particle volume fraction	% bulk depletion[b]	τ (h) [c]	$D_{X,p}$ (m^2 s^{-1}) [d]	NRMSE, kinetic fitting [c,e]	equilibrium isotherm [f]	Ref
PE	fluoranthene	1×10^{-4}	1.5×10^{-3}	79.9	2276.3 (1529.4 – 3023.3)	1.22×10^{-15}	0.044 [$K^{L}_{p,w}$ varied: 1.781×10^{4} (1.331×10^{4} – 2.231×10^{4})]	Langmuir $c^{max,s}_{X,p}$ =0.28 $K^{L}_{p,w}$ =8.755×10^{4} NRMSE=0.101	40
PE	fluoranthene	5.45×10^{-4}	1.5×10^{-3}	70.9	4354.9 (2908.8 – 5801.1)	1.90×10^{-14}	0.080	Langmuir $c^{max,s}_{X,p}$ =0.24 $K^{L}_{p,w}$ =1.456×10^{4} NRMSE=0.113	40
PE	fluoranthene	2.485×10^{-5} – 1.295×10^{-4}	3.333×10^{-4}	92.8	139.6 (66.9 – 212.2)	1.23×10^{-15} (24.85 µm) 3.34×10^{-14} (129.5 µm)	0.048 [$K^{L}_{p,w}$ varied: 3.021×10^{4} (2.72×10^{3} – 5.771×10^{4})]	Langmuir $c^{max,s}_{X,p}$ =2.66 $K^{L}_{p,w}$ =9325.9 NRMSE=0.052	5
PE	fluoranthene	1.5×10^{-3}	6.667×10^{-4}	91.9	162.9 (134.8 – 190.9)	3.84×10^{-12}	0.027 [$K^{L}_{p,w}$ varied: 2.042×10^{5} (2.096×10^{4} – 3.793×10^{5})]	Langmuir $c^{max,s}_{X,p}$ =0.77 $K^{L}_{p,w}$ =5.875×10^{4} NRMSE=0.045	5
PET	fluoranthene	1.5×10^{-3}	6.667×10^{-4}	93.4	937.4 (499.4 – 1375.4)	6.67×10^{-13}	0.024 [$K^{L}_{p,w}$ varied: 8730.4 (4132.7 – 13328.0)]	Langmuir $c^{max,s}_{X,p}$ =3.41 $K^{L}_{p,w}$ =7075.3 NRMSE=0.039	5
PE	phenanthrene	5.45×10^{-4}	1.5×10^{-3}	62.8	2.294×10^{4} (1.844×10^{4} – 2.744×10^{4})	3.60×10^{-15}	0.062 (5^{th} data point omitted)	Langmuir $c^{max,s}_{X,p}$ =0.17 $K^{L}_{p,w}$ =2680.3 NRMSE=0.039	40
PE	napthalene	2.485×10^{-5} – 1.295×10^{-4}	3.333×10^{-4}	67.4	486.9 (203.7 – 770.2)	3.52×10^{-16} (24.85 µm) 9.57×10^{-15} (129.5 µm)	0.048 [$K^{L}_{p,w}$ varied: 3161.0 (1768.5 – 4553.5)]	Langmuir $c^{max,s}_{X,p}$ =3.68 $K^{L}_{p,w}$ =2312.7 NRMSE=0.046	5

polymer[a]	compound, X	particle radius, a (m)	particle volume fraction	% bulk depletion[b]	τ (h) [c]	$D_{X,p}$ (m^2 s^{-1}) [d]	NRMSE, kinetic fitting [c,e]	equilibrium isotherm [f]	Ref
PE	napthalene	1.5×10^{-3}	6.667×10^{-4}	59.2	114.8 (75.2 – 154.4)	5.45×10^{-12}	0.060	Langmuir $c_{X,p}^{max,s}$ =0.69 $K_{p,w}^{L}$ =1.210×10^{5} NRMSE=0.107	5
PET	napthalene	1.5×10^{-3}	6.667×10^{-4}	87.2	2225.2 (1833.3 – 2617.1)	2.81×10^{-13}	0.038	Langmuir $c_{X,p}^{max,s}$ =3.39 $K_{p,w}^{L}$ =5268.2 NRMSE=0.067	5
PLA	napthalene	1.5×10^{-3}	6.667×10^{-4}	21.4	173.3 (101.7 – 244.9)	3.61×10^{-12}	0.070	Langmuir $c_{X,p}^{max,s}$ =0.25 $K_{p,w}^{L}$ =2.453×10^{4} NRMSE=0.034	5
PE	1-methyl-naphthalene	9×10^{-5}	5×10^{-3}	89.3	34.0 (14.0 – 54.0)	6.62×10^{-14}	0.025 [$K_{p,w}^{H}$ varied: 1726.8 (1296.9 – 2156.7)]	Henry $K_{p,w}^{H}$ =1230.9 NRMSE=0.031	41
PE	fluorene	2.485×10^{-5} – 1.295×10^{-4}	3.333×10^{-4}	50.9	145.5 (111.7 – 179.3)	1.18×10^{-15} (24.85 µm) 3.20×10^{-14} (129.5 µm)	0.018 [$K_{p,w}^{L}$ varied: 703.9 (645.5 – 762.4)]	Langmuir $c_{X,p}^{max,s}$ =5.34 $K_{p,w}^{L}$ =975.4 NRMSE=0.038	5
PE	fluorene	1.5×10^{-3}	6.667×10^{-4}	48.4	177.9 (115.8 – 239.9)	3.51×10^{-12}	0.043 [$K_{p,w}^{L}$ varied: 8275.6 (5514.8 – 11036.4)]	Langmuir $c_{X,p}^{max,s}$ =0.61 $K_{p,w}^{L}$ =4.199×10^{4} NRMSE=0.103	5
PET	fluorene	1.5×10^{-3}	6.667×10^{-4}	62.7	213.7 (121.8 – 305.5)	2.93×10^{-12}	0.040 [$K_{p,w}^{L}$ varied: 1875.1 (1492.5 – 2257.8)]	Langmuir $c_{X,p}^{max,s}$ =1.91 $K_{p,w}^{L}$ =1.218×10^{4} NRMSE=0.042	5

polymer[a]	compound, X	particle radius, a (m)	particle volume fraction	% bulk depletion[b]	τ (h) [c]	$D_{X,p}$ (m^2 s^{-1}) [d]	NRMSE, kinetic fitting [c,e]	equilibrium isotherm [f]	Ref
PP	fluorene	1.5×10^{-3}	6.667×10^{-4}	76.6	292.7 (138.7 – 446.8)	2.14×10^{-12}	0.066 [$K^{L}_{p,w}$ varied: 1.959×10^{4} (2.898×10^{3} – 3.628×10^{4})]	Langmuir $c^{max,s}_{X,p}$ =0.95 $K^{L}_{p,w}$ =1.111×10^{4} NRMSE=0.031	5
PLA	fluorene	1.5×10^{-3}	6.667×10^{-4}	22.7	319.2 (154.9 – 483.6)	1.96×10^{-12}	0.049 [$K^{L}_{p,w}$ varied: 5154.8 (2674.8 – 7634.7)]	Langmuir $c^{max,s}_{X,p}$ =0.30 $K^{L}_{p,w}$ =6718.5 NRMSE=0.067	5
PE	fluorene	9×10^{-5}	5×10^{-3}	55.5	11.0 (9.1 – 13.0)	2.04×10^{-13}	0.082	Langmuir $c^{max,s}_{X,p}$ = 13.42 $K^{L}_{p,w}$ =541.9 NRMSE=0.041	42
PE	dibenzothiophene	9×10^{-5}	5×10^{-3}	76.5	4.6 (3.6 – 5.7)	4.85×10^{-13}	0.063 [$K^{L}_{p,w}$ varied: 168.8 (119.6 – 217.9)]	Langmuir $c^{max,s}_{X,p}$ =19.05 $K^{L}_{p,w}$ =114.4 NRMSE=0.028	42
PE	dibenzofuran	9×10^{-5}	5×10^{-3}	48.1	6.6 (5.1 – 8.1)	3.42×10^{-13}	0.057 [$K^{L}_{p,w}$ varied: 45.9 (37.7 – 54.0)]	Langmuir $c^{max,s}_{X,p}$ = 13.59 $K^{L}_{p,w}$ =121.7 NRMSE=0.035	42
PS	pyrene	3.75×10^{-5} – 7.5×10^{-5}	3.333×10^{-4}	68.5	470.9 (347.0 – 594.8)	8.30×10^{-16} (37.5 µm) 3.32×10^{-15} (75 µm)	0.037	Langmuir $c^{max,s}_{X,p}$ =2.60 $K^{L}_{p,w}$ =3038.3 NRMSE=0.003	43
PE	pyrene	2.485×10^{-5} – 1.295×10^{-4}	3.333×10^{-4}	65.6	460.9 (213.9 – 707.9)	3.72×10^{-16} (24.85 µm) 1.01×10^{-14} (129.5 µm)	0.024 [$K^{L}_{p,w}$ varied; omitted 2nd and 3rd data points: 1702.1 (1291.4 – 2112.8)]	Langmuir $c^{max,s}_{X,p}$ =4.47 $K^{L}_{p,w}$ =2.505×10^{4} NRMSE=0.047	5

polymer[a]	compound, X	particle radius, a (m)	particle volume fraction	% bulk depletion[b]	τ (h) [c]	$D_{X,p}$ (m^2 s^{-1}) [d]	NRMSE, kinetic fitting [c,e]	equilibrium isotherm [f]	Ref
PE	pyrene	1.5×10^{-3}	6.667×10^{-4}	92.3	366.0 (296.0 – 436.0)	1.71×10^{-12}	0.038	Langmuir $c_{X,p}^{max,s}$ =1.02 $K_{p,w}^{L}$ =5.442×10^{4} NRMSE=0.043	5
PET	pyrene	1.5×10^{-3}	6.667×10^{-4}	93.3	536.7 (272.1 – 801.3)	1.17×10^{-12}	0.035 [$K_{p,w}^{L}$ varied: 1.406×10^{4} (4.365×10^{3} – 2.376×10^{4})]	Langmuir $c_{X,p}^{max,s}$ =2.22 $K_{p,w}^{L}$ =5.982×10^{4} NRMSE=0.048	5
PLA	pyrene	1.5×10^{-3}	6.667×10^{-4}	31.0	183.0 (83.1 – 282.9)	3.42×10^{-12}	0.069 [$K_{p,w}^{L}$ varied: 1.906×10^{4} (350.5 – 3.777×10^{4})]	Langmuir $c_{X,p}^{max,s}$ =0.27 $K_{p,w}^{L}$ =2.626×10^{4} NRMSE=0.034	5
PS	benzophenone-3	2.5×10^{-7}	6.667×10^{-4}	25.4	60.1 (52.9 – 67.2)	2.89×10^{-19}	0.019	Langmuir $c_{X,p}^{max,s}$ =0.42 $K_{p,w}^{L}$ =6147.2 NRMSE=0.013	7
PS	benzophenone-3	2.5×10^{-6}	6.667×10^{-4}	22.1	67.8 (46.9 – 88.8)	2.56×10^{-17}	0.050	Langmuir $c_{X,p}^{max,s}$ =0.39 $K_{p,w}^{L}$ =4416.8 NRMSE=0.018	7
PS	benzophenone-3	3.75×10^{-5}	6.667×10^{-4}	17.8	55.0 (37.5 – 72.6)	7.10×10^{-15}	0.051	Langmuir $c_{X,p}^{max,s}$ =0.34 $K_{p,w}^{L}$ =3183.7 NRMSE=0.023	7
PS	benzophenone-3	1.25×10^{-4}	6.667×10^{-4}	13.9	126.8 (90.6 – 163.0)	3.42×10^{-14}	0.048	Langmuir $c_{X,p}^{max,s}$ =0.27 $K_{p,w}^{L}$ =2958.1 NRMSE=0.025	7

polymer[a]	compound, X	particle radius, a (m)	particle volume fraction	% bulk depletion[b]	τ (h) [c]	$D_{X,p}$ (m^2 s^{-1}) [d]	NRMSE, kinetic fitting [c,e]	equilibrium isotherm [f]	Ref
PS	benzophenone-3	2.75×10^{-4}	6.667×10^{-4}	10.9	207.4 (103.3 – 311.4)	1.01×10^{-13}	0.070	Langmuir $c_{X,p}^{max,s}$ =0.23 $K_{p,w}^{L}$ =2383.5 NRMSE=0.024	7
PE	benzophenone-3	3.75×10^{-5}	6.667×10^{-4}	11.7	56.1 (44.2 – 68.0)	6.96×10^{-15}	0.029 (omitted 6th data point)	LF, p_{LF}=1.37; $c_{X,p}^{max,s}$ =0.244 $K_{p,w}^{LF}$ =2660.0 NRMSE=0.016	7
PE	benzophenone-3	1.25×10^{-4}	6.667×10^{-4}	10.2	74.3 (64.1 – 84.5)	5.84×10^{-14}	0.022	LF, p_{LF} =1.24; $c_{X,p}^{max,s}$ =0.21 $K_{p,w}^{LF}$ =2422.7 NRMSE=0.020	7
PE	benzophenone-3	2.75×10^{-4}	6.667×10^{-4}	6.3	108.5 (69.1 – 147.8)	1.94×10^{-13}	0.059	Langmuir $c_{X,p}^{max,s}$ = 0.11 K_{L} = 3296.5 NRMSE=0.021	7
PP	benzophenone-3	3.75×10^{-5}	6.667×10^{-4}	13.0	34.8 (21.8 – 47.9)	1.12×10^{-14}	0.061	Langmuir $c_{X,p}^{max,s}$ =0.24 $K_{p,w}^{L}$ =3015.4 NRMSE=0.031	7
PP	benzophenone-3	1.25×10^{-4}	6.667×10^{-4}	9.0	41.3 (24.3 – 58.3)	1.05×10^{-13}	0.067	Langmuir $c_{X,p}^{max,s}$ =0.18 $K_{p,w}^{L}$ =2515.5 NRMSE=0.030	7
PP	benzophenone-3	2.75×10^{-4}	6.667×10^{-4}	4.4	66.3 (38.0 – 94.6)	3.17×10^{-13}	0.070	LF, p=1.329 $c_{X,p}^{max,s}$ =0.16 $K_{p,w}^{LF}$ =541.9 NRMSE=0.023	7

polymer[a]	compound, X	particle radius, a (m)	particle volume fraction	% bulk depletion[b]	τ (h) [c]	$D_{X,p}$ (m^2 s^{-1}) [d]	NRMSE, kinetic fitting [c,e]	equilibrium isotherm [f]	Ref
PA	tebuconazole	3.7×10^{-5} – 7.5×10^{-5}	1×10^{-3}	18.5	29.1 (24.1 – 34.2)	1.31×10^{-14} (37 µm) 5.36×10^{-14} (75 µm)	0.018 [$K^{L}_{p,w}$ varied: 4.0 (3.8 – 4.1)]	Langmuir $c^{max,s}_{X,p}$ =60.34 $K^{L}_{p,w}$ =9.8 NRMSE=0.017	44
PS	tebuconazole	3.7×10^{-5} – 7.5×10^{-5}	1×10^{-3}	14.5	53.2 (41.3 – 65.0)	7.15×10^{-15} (37 µm) 2.94×10^{-14} (75 µm)	0.025 [$K^{L}_{p,w}$ varied: 15.6 (14.7 – 16.4)]	Langmuir $c^{max,s}_{X,p}$ =13.26 $K^{L}_{p,w}$ =36.3 NRMSE=0.026	44
PP	tebuconazole	3.7×10^{-5} – 7.5×10^{-5}	1×10^{-3}	14.1	85.9 (51.5 – 120.2)	4.43×10^{-15} (37 µm) 1.82×10^{-14} (75 µm)	0.043 [$K^{L}_{p,w}$ varied: 20.5 (18.2 – 22.8)]	Langmuir $c^{max,s}_{X,p}$ =10.28 $K^{L}_{p,w}$ =39.4 NRMSE=0.010	44
PVC	1H-benzotriazole (BTR)	1×10^{-7}	1.5×10^{-3}	47.7	114.2 (101.5 – 127.0)	2.43×10^{-20}	0.024	Langmuir $c^{max,s}_{X,p}$ =3.70 $K^{L}_{p,w}$ =196.2 NRMSE=0.034	45
PVC	1-hydroxy-benzotriazole (1-OH-BTR)	1×10^{-7}	1.5×10^{-3}	27.3	57.0 (45.9 – 68.1)	4.87×10^{-20}	0.023 [$K^{L}_{p,w}$ varied: 412.4 (387.8 – 436.9)]	Langmuir $c^{max,s}_{X,p}$ =0.88 $K^{L}_{p,w}$ =518.2 NRMSE=0.042	45
PVC	5-methyl-1H-benzotriazole (5TTR)	1×10^{-7}	1.5×10^{-3}	52.8	109.4 (100.0 – 118.8)	2.54×10^{-20}	0.018	Langmuir $c^{max,s}_{X,p}$ =2.36 $K^{L}_{p,w}$ =411.9 NRMSE=0.039	45
PVC	5,6-dimethyl-1H-benzotriazole (XTR)	1×10^{-7}	1.5×10^{-3}	60.1	72.4 (67.4 – 77.5)	3.83×10^{-20}	0.013	Langmuir $c^{max,s}_{X,p}$ =1.94 $K^{L}_{p,w}$ =719.2 NRMSE=0.032	45

polymer[a]	compound, X	particle radius, a (m)	particle volume fraction	% bulk depletion[b]	τ (h) [c]	$D_{X,p}$ (m^2 s^{-1}) [d]	NRMSE, kinetic fitting [c,e]	equilibrium isotherm [f]	Ref
PVC	5-chloro-1H-benzotriazole (5Cl1HBTR)	1×10^{-7}	1.5×10^{-3}	54.1	81.8 (73.1 – 90.5)	3.40×10^{-20}	0.020	Langmuir $c_{X,p}^{max,s}$ =2.60 $K_{p,w}^{L}$ =369.4 NRMSE=0.032	45
PVC	2-hydroxy-benzothiazole (2OHBTH)	1×10^{-7}	1.5×10^{-3}	68.6	127.0 (115.4 – 138.7)	2.19×10^{-20}	0.017	Langmuir $c_{X,p}^{max,s}$ =3.29 $K_{p,w}^{L}$ =551.2 NRMSE=0.040	45
PVC	2-methylthio-benzothiazole (2MeSBTH)	1×10^{-7}	1.5×10^{-3}	74.5	117.8 (112.6 – 122.9)	2.36×10^{-20}	0.008	Langmuir $c_{X,p}^{max,s}$ =1.94 $K_{p,w}^{L}$ =1416.1 NRMSE=0.044	45
PVC	2-amine-benzothiazole (2NH2BTH)	1×10^{-7}	1.5×10^{-3}	56.2	76.0 (70.9 – 81.1)	3.65×10^{-20}	0.013	Langmuir $c_{X,p}^{max,s}$ =2.45 $K_{p,w}^{L}$ =438.7 NRMSE=0.042	45
PA6	methyl orange	3.75×10^{-5} – 7.5×10^{-5}	1×10^{-3}	67.8	346.4 (197.8 – 495.1)3.1	1.13×10^{-15} (37.5 µm) 4.51×10^{-15} (75 µm)	0.045 [$K_{p,w}^{L}$ varied: 190.5 (88.3 – 292.8)]	Langmuir $c_{X,p}^{max,s}$ =33.25 $K_{p,w}^{L}$ =96.8 NRMSE=0.035	46
PA66	methyl orange	3.75×10^{-5} – 7.5×10^{-5}	1×10^{-3}	43.8	260.3 (166.4 – 354.1)	1.50×10^{-15} (37.5 µm) 6.00×10^{-15} (75 µm)	0.035 [$K_{p,w}^{L}$ varied: 60.9 (46.5 – 75.2)]	Langmuir $c_{X,p}^{max,s}$ =26.85 $K_{p,w}^{L}$ =43.6 NRMSE=0.026	46
PA66	malachite green	3.75×10^{-5} – 7.5×10^{-5}	1×10^{-3}	24.7	125.1 (108.4 – 141.8)	3.12×10^{-15} (37.5 µm) 1.25×10^{-14} (75 µm)	0.026	Langmuir $c_{X,p}^{max,s}$ =14.20 $K_{p,w}^{L}$ =44.1 NRMSE=0.013	46

polymer[a]	compound, X	particle radius, a (m)	particle volume fraction	% bulk depletion[b]	τ (h) [c]	$D_{X,p}$ (m^2 s^{-1}) [d]	NRMSE, kinetic fitting [c,e]	equilibrium isotherm [f]	Ref
PE	cyhalothrin	2.5×10^{-6}	1×10^{-4}	35.9	217.2 (112.5 – 322.0)	7.99×10^{-18}	0.055 [$K^{L}_{p,w}$ varied: 165.3 (85.2 – 245.5)]	Langmuir $c^{max,s}_{X,p}$ =115.40 $K^{L}_{p,w}$ =126.5 NRMSE=0.025	47

[a] PS = polystyrene; PVC = polyvinyl chloride; PLA = polylactic acid, PU = polyurethane; PP = polypropylene; PE = polyethylene; PBAT = polybutylene adipate terephthalate; PET = polyethylene terephthalate; PA = polyamide; PBS = polybutylene succinate.

[b] extent to which the concentration of X in the bulk aqueous medium is depleted at the final time point in the kinetic sorption curve

[c] in parentheses, lower and upper 95% confidence limits, see main text for details

[d] when a range of particle radii is reported, $D_{X,p}$ was computed for the lowest and highest values (pertaining a given in brackets)

[e] unless otherwise stated, the equilibrium constant is fixed at the value determined independently from the equilibrium isotherm

[f] $K^{H}_{p,w}$, dimensionless; $K^{L}_{p,w}$ and $K^{LF}_{p,w}$, m^3 mol^{-1}; $c^{max,s}_{X,p}$, mol m^{-3}; p_{LF}, dimensionless. LF = Langmuir-Freundlich

References

1 M. Jiang, L. Hu, A. Lu, G. Liang, Z. Lin, T. Zhang, L. Xu, B. Li and W. Gong, Strong sorption of two fungicides onto biodegradable microplastics with emphasis on the negligible role of environmental factors, *Environ. Poll.*, 2020, **267**, 115496.

2 L. Wang, H. Yang, M. Guo, Z. Wang and X. Zheng, Adsorption of antibiotics on different microplastics (MPs): behavior and mechanism, *Sci. Total Environ.*, 2023, **863**, 161022.

3 R. A. Funari, L. M. Frescura, B. B. de Menezes, A. F. de Moraes Bastos and M. B. da Rosa, Adsorption of naphthalene and its derivatives onto high-density polyethylene microplastic: computational, isotherm, thermodynamic, and kinetic study, *Environ. Poll.*, 2023, **318**, 120919.

4 Y. Zhang, Z. Chen, Y. Shi, Q. Ma, H. Mao, Y. Li, H. Wang and Y. Zhang, Revealing the sorption mechanisms of carbamazepine on pristine and aged microplastics with extended DLVO theory, *Sci. Total Environ.*, 2023, **874**, 162480.

5 M. Lončarski, V. Gvoić, M. Prica, L. Cveticanin, J. Agbaba and A. Tubič, Sorption behavior of polycyclic aromatic hydrocarbons on biodegradable polylactic acid and various nondegradable microplastics: model fitting and mechanism analysis, *Sci. Total Environ.*, 2021, **785**, 147289.

6 J. Fei, J. Cui, B. Wang, H. Xie, C. Wang, Y. Zhao, H. Sun and X. Yin, Co-transport of degradable microplastics with Cd(II) in saturated porous media: synergistic effects of strong adsorption affinity and high mobility, *Environ. Poll.*, 2023, **330**, 121804.

7 R. Cui, M. -C. Jong, L. You, F. Mao, D. Yao, K. Y. -H. Gin and Y. He, Size dependent adsorption of waterborne benzophenone-3 on microplastics and its desorption under simulated gastrointestinal conditions, *Chemosphere*, 2022, **286**, 131735.

8 Y. Zhou, Y. Yang, G. Liu, G. He and W. Liu, Adsorption mechanism of cadmium on microplastics and their desorption behavior in sediment and gut environments: the roles of water pH, lead ions, natural organic matter and phenanthrene, *Water Res.*, 2020, **184**, 116209.

9 S. E. Hale, T. J. Martin, K. -U. Goss, H. P. H. Arp and D. Werner, Partitioning of organochlorine pesticides from water to polyethylene passive samplers, *Environ. Poll.*, 2010, **158**, 2511-2517.

10 F. C. Fischer, O. A. Cirpka, K. -U. Goss, L. Henneberger and B. I. Escher, Application of experimental polystyrene partition constants and diffusion coefficients to predict the sorption of neutral organic chemicals to multiwell plates in in vivo and in vitro bioassays, *Environ. Sci. Technol.*, 2018, **52**, 13511-13522.

11 F. Fornasiero, M. M. Olaya, B. Esprester, V. Nguyen and J. M. Prausnitz, Diffusion coefficients and diffusivities in three polymers for nineteen aqueous nonvolatile solutes, *J. Appl. Polym. Sci.*, 2002, **85**, 2041-2052.

12 H. P. Sangam and R. K. Rowe, Migration of dilute aqueous organic pollutants through HDPE geomembranes, *Geotext. Geomem.*, 2001, **19**, 329-357.

13 M. Saleem, A. A. Asfour and D. De Kee, Diffusion of organic penetrants through low density polyethylene (LDPE) films: effect of size and shape of the penetrant molecule, *J. Appl. Polym. Sci.*, 1989, **37**, 617-625.

14 I. S. Voultzatis, C. D. Papaspyrides, C. J. Tsenoglou and C. Roussis, Diffusion of model contaminants in high-density polyethylene, *Macromol. Mater. Eng.*, 2007, **292**, 272-284.

15 Y. Zhou, L. Hou, H. Chen, R. Steenbakkers, K. Sehanobish, P. Wu and Q. Shi, FT-IR studies of factors affecting the diffusivitiy of oligo (oxyethylene) fatty acid ester in PE films: effect of temperature, ethylene oxide chain length and base resin type, *Polymer*, 2017, **130**, 150-160.

16 D. Klose, F. Siepmann, K. Elkharraz and J. Siepmann, PLGA-based drug delivery systems: importance of the type of drug and device geometry, *Int. J. Pharm.*, 2008, **354**, 95-103.

17 J. M. Saquing, C. D. Saquing, D. R. U. Knappe and M. A. Barlaz, Impact of plastics on fate and transport of organic contaminants in landfills, *Environ. Sci. Technol.*, 2010, **44**, 6396-6402.

18 S. Seidensticker, C. Zarfl, O. A. Cirpka and P. Grathwohl, Microplastic-contaminant interactions: influence of nonlinearity and coupled mass transfer, *Environ. Toxicol. Chem.*, 2019, **38**, 1635-1644.

19 H. K. Karapanagoti and I. Klontza, Testing phenanthrene distribution properties of virgin plastic pellets and plastic eroded pellets found on Lesvos island beaches (Greece), *Mar. Environ. Res.*, 2008, **65**, 283-290.

20 R. M. Town, H. P. van Leeuwen and J. F. L. Duval, Effect of polymer aging on uptake/release kinetics of metal ions and organic molecules by micro- and nanoplastics: implications for the bioavailability of the associated compounds, *Environ. Sci. Technol.*, 2023, **57**, 16552-16563.

21 L. Gao, D. Fu, J. Zhao, W. Wu, Z. Wang, Y. Su and L. Peng, Microplastics aged in various environmental media exhibited strong sorption to heavy metals in seawater, *Mar. Poll. Bull.*, 2021, **169**, 112480.

22 T. Li, X. Cao, X. Cui, R. Zhao, H. Chen, W. Xue, Z. Cui, X. Tan and S. Ni, Competitive adsorption of lead and cadmium onto nanoplastics with different charges: two-dimensional correlation spectroscopy study, *Environ. Sci. Poll. Res.*, 2023, **30**, 72884-72899.

23 X. -D. Xue, C. -R. Fang and H. -F. Zhuang, Adsorption behaviors of the pristine and aged thermoplastic polyurethane microplastics in Cu(II)-OTC coexisting system, *J. Haz. Mater.*, 2021, **407**, 124835.

24 W. Huang, J. Zhang, Z. Zhang, H. Gao, W. Xu and X. Xia, Insights into adsorption behavior and mechanism of Cu(II) onto biodegradable and conventional microplastics: effect of aging process and environmental factors, *Environ. Poll.*, 2024, **342**, 123061.

25 A. Sun, L. Xu, G. Zhou, E. Yin, T. Chen, Y. Wang and X. Li, Roles of polystyrene micro/nano-plastics as carriers on the toxicity of Pb^{2+} to *Chlamydomonas reinhardtii*, *Chemosphere*, 2022, **309**, 136676.

26 X. Liu, J. Zhang, W. Cao, Y. Hu and W. Shen, The influence of Pb(II) adsorption on (non)biodegradable microplastics by UV/O_3 oxidation treatment, *J. Environ. Chem. Eng.*, 2022, **10**, 108615.

27 C. Guo, L. Wang, D. Lang, Q. Qian, W. Wang, R. Wu and J. Wang, UV and chemical aging alter the adsorption behavior of microplastics for tetracycline, *Environ. Poll.*, 2023, **318**, 120859.

28 C. Chen, X. Pang, Q. Chen, M. Xu, Y. Xiao, J. Wu, Y. Zhang, Y. Liu, L. Long and G. Yang, Tetracycline adsorption trajectories on aged polystyrene in a simulated aquatic environment: a mechanistic investigation, *Sci. Total Environ.*, 2022, **851**, 158204.

29 F. Yu, C. Yang, G. Huang, T. Zhou, Y. Zhao and J. Ma, Interfacial interaction between diverse microplastics and tetracycline by adsorption in an aqueous solution, *Sci. Total Environ.*, 2020, **721**, 137729.

30 H. Wang, C. Qiu, Y. Song, S. Bian, Q. Wang, Y. Chen and C. Fang, Adsorption of tetracycline and Cd(II) on polystyrene and polyethylene terephthalate microplastics with ultraviolet and hydrogen peroxide aging treatment, *Sci. Total Environ.*, 2022, **845**, 157109.

31 F. Tong, D. Liu, Z. Zhang, W. Chen, G. Fan, Y. Gao, X. Gu and C. Gu, Heavy metal-mediated adsorption of antibiotic tetracycline and ciprofloxacin on two microplastics: insights into the role of complexation, *Environ. Res.*, 2023, **216**, 114716.

32 Y. Tian, J. Zhu, C. Ying, H. Luo, S. Zhang, L. Zhang, R. Li and J. Li, Photoaging processes of polyvinyl chloride microplastics enhance the adsorption of tetracycline and facilitate the formation of antibiotic resistance, *Chemosphere*, 2023, **320**, 137820.

33 K. Wang, T. Han, X. Chen, L. E. Rushimisha, Y. Liu, S. Yang, X. Miao, X. Li, L. Weng and Y. Li, Insights into behavior and mechanism of tetracycline adsorption on virgin and soil-exposed microplastics, *J. Haz. Mater.*, 2022, **440**, 129770.

34 F. Kong, X. Xu, Y. Xue, Y. Gao, L. Zhang, L. Wang, S. Jiang and Q. Zhang, Investigation of the adsorption of sulfamethoxazole by degradable microplastics artificially aged by chemical oxidation, *Arch. Environ. Contamin. Toxicol.*, 2021, **81**, 155-165.

35 G. Liu, Z. Zhu, Y. Yang, Y. Sun, F. Yu, J. Ma, Sorption behavior and mechanism of hydrophilic organic chemicals to virgin and aged microplastics in freshwater and seawater, *Environ. Poll.*, 2019, **246**, 26-33.

36 Y. Wang, C. Liu, F. Wang and Q. Sun, Behavior and mechanism of atrazine adsorption on pristine and aged microplastics in the aquatic environment: kinetic and thermodynamic studies, *Chemosphere*, 2022, **292**, 133425.

37 W. Liu, T. Pan, H. Liu, M. Jiang and T. Zhang, Adsorption behavior of imidacloprid pesticide on polar microplastics under environmental conditions: critical role of photo-aging, *Front. Environ. Sci. Eng.*, 2023, **17**, 41.

38 J. Ma, J. Zhao, Z. Zhu, L. Li and F. Yu, Effect of microplastic size on the adsorption behavior and mechanism of triclosan on polyvinyl chloride, *Environ. Poll.*, 2019, **254**, 113104.

39 W. Gong, M. Jiang, P. Han, G. Liang, T. Zhang and G. Liu, Comparative analysis on the sorption kinetics and isotherms of fipronil on nondegradable and biodegradable microplastics, *Environ. Poll.*, 2019, **254**, 112927.

40 F. A. O. Udenby, H. Almuhtaram, M. J. McKie and R. C. Andrews, Adsorption of fluoranthene and phenanthrene by virgin and weathered polyethylene microplastics in freshwaters, *Chemosphere*, 2022, **307**, 135585.
41 R. A. Funari, L. M. Frescura, B. B. de Menezes, A. F. de Moraes Bastos and M. B. da Rosa, Adsorption of naphthalene and its derivatives onto high-density polyethylene microplastic: computational, isotherm, thermodynamic, and kinetic study, *Environ. Poll.*, 2023, **318**, 120919.
42 L. M. Frescura, R. A. Funari, B. B. de Menezes, A. F. de Moreas Bastos and M. B. da Rosa, Interaction of fluorene and its analogs with high-density polyethylene microplastics: an assessment of the adsorption mechanism to establish the effects of heteroatoms in the molecule, *Environ. Poll.*, 2023, **337**, 122573.
43 C. Yang, W. Wu, X. Zhou, Q. Hao, T. Li and Y. Liu, Comparing the sorption of pyrene and its derivatives onto polystyrene microplastics: insights from experimental and computational studies, *Mar. Poll. Bull.*, 2021, **173**, 113086.
44 N. Cui, P. Wang and N. Xu, Sorption behaviour of tebuconazole on microplastics: kinetics, isotherms and influencing factors, *Environ. Technol.*, 2023, **44**, 3937-3948.
45 Y. Yu, H. Li, J. Chen, F. Wang, X. Chen, B. Huang, Y. He and Z. Cai, Exploring the adsorption behavior of benzotriazoles and benzothiazoles on polyvinyl chloride microplastics in the water environment, *Sci. Total Environ.*, 2022, **821**, 153471.
46 K. Wang, Y. Kou, K. Wang, S. Liang, C. Guo, W. Wang, Y. Lu, and Y. Wang, Comparing the adsorption of methyl orange and malachite green on similar yet distinct polyamide microplastics: uncovering hydrogen bond interactions, *Chemosphere*, 2023, **340**, 139806.
47 Y. Zhao, H. Chen, H. Liang, T. Zhao, B. Ren, Y. Li, H. Liang, Y. Liu, H. Cao, N. Cui and W. Wei, Combined toxic effects of polyethylene microplastics and lambda-cyhalothrin on gut of zebrafish (*Danio rerio*), *Ecotoxicol. Environ. Safety*, 2024, **276**, 116296.